Synthesis, characterization, and nitrite reductase activity of Ni(II) Complexes

A Thesis submitted to

Indian Institute of Science Education and Research (IISER), PUNE

In partial fulfillment of the requirements for the M.Sc. Degree Programme

By

Arijit Panja

(M.Sc. student; Registration No: 20226214**)**

Under the supervision of

Dr. Debangsu Sil
Assistant professor
Indian Institute of Science Education and Research
Pune, 411008, India

Certificate

This is to certify that this dissertation entitled “Synthesis, characterization, and nitrite reductase activity of Ni(II) complexes” towards the partial fulfilment of the M.Sc. degree program at the Indian Institute of Science Education and Research, Pune represents the research work carried out by Arijit Panja under the supervision of Dr. Debangsu Sil, Assistant Professor, Department of Chemistry, during the academic year 2023-2024.

Digitally signed by Debangsu Sil
DN: cn=Debangsu Sil, o=IISER Pune, ou, email=debangsu@iiserpune.ac.in, c=IN
Date: 2024.04.12 17:22:28 +05'30'

Dr. Debangsu Sil

Committee:

Dr. Debangsu Sil

Prof. Sujit Ghosh

This thesis is dedicated
to
my parents and my supervisor

Declaration

I hereby declare that the matter embodied in the report entitled “Synthesis, characterization, and nitrite reductase activity of Ni(II) complexes” are the results of the work carried out by me at the Department of Chemistry, Indian Institute of Science Education and Research, Pune, under the supervision of Dr. Debangsu Sil and the same has not been submitted elsewhere for any other degree.

Arijit Panja

Date: 12th April, 2024

Acknowledgments

I would like to express my gratitude towards all the individuals who contributed in some way to the research work described in this thesis. Above all, I want to thank my academic mentor, Dr. Debangsu Sil, for accepting me into his group. Throughout my tenure, he provided me with intellectual freedom, introduced me to new ideas, and expected a high standard of work in all my endeavors. Moreover, I would like to thank my thesis expert, Professor Sujit Ghosh, for his valuable suggestions during my review meeting.

All the results presented in this thesis were achieved with the generous contributions and support of my fellow labmates. When I first joined the lab as an undergraduate, Somsubhra provided me with invaluable assistance for my project. Without his efforts, my job would have undoubtedly been much more difficult. I am particularly grateful for his scientific insight and his ability to explain complex ideas in simple terms. I would also like to express my appreciation to all the members of the lab, including Soumojyati, Anirban, Suneel, Manju, and Akanksha, for their unwavering support and excellent collaboration throughout the entire project.

I would like to express my gratitude to the Department of Chemistry at IISER Pune for the outstanding undergraduate experience that I had. The department offered excellent courses and seminars that added great value to my academic journey.

Finally, I would like to express my gratitude towards my friends and family who have supported me throughout my time here at IISER. First and foremost, I would like to thank my Mom and Dad for their constant love and support. I would be remiss if I did not thank Supravat da, who deserves credit for providing much-needed assistance. I also want to thank Sovik da, Rahul da, Somnath da, Animesh da, Ankan, Hritwik, Sayandip, and other members of the "IN-N-OUT" group who made my time at IISER a lot more enjoyable and memorable.

Abbreviations

Chemical Abbreviation		Units, Standard terms, and general notations	
ACN	Acetonitrile	*J*	Coupling constant in NMR
Ar	Aryl	HRMS	High Resolution Mass Spectrometry
$CDCl_3$	Deuterated chloroform		
DMSO-d_6	Deuterated Dimethyl sulfoxide	NMR	Nuclear Magnetic resonance
DCM	Dichloromethane	UV	Ultra-Violate
MeOH	Methanol	δ	Chemical shift
EtOH	Ethanol	ppm	parts per million
DMF	Dimethylformamide	SC-XRD	Single Crystal X-Ray Diffraction
PMe_3	Trimethyl phosphine	Hz	Hertz
R_2S	Thioether	λ	wavelength
RSH	Thiol	^0C	Degree centigrade
KBr	Potassium bromide	FTIR	Fourier Transform Infrared spectroscopy
NO	Nitric oxide		
$NaNO_2$	Sodium nitrite	mg	milligram
$NaNO_3$	Sodium nitrate	h	Hour
Nu	Nucleophile	mmol	millimole

List of Schemes

:

Abstract

In biological systems, different types of nitrite reductase (NiRs) and nitric oxide synthase (NOS) isozymes are present to generate NO for physiological activities. To mimic this function, we choose the acid-induced path to reduced nitrite for nickel-nitrite metal complexes. In this study, we utilized the $(BimH)_3$ ligand framework and synthesized three different complexes, namely $[(BimH)_3Ni^{II}(\mu\text{-}Cl)_2Ni^{II}(BimH)_3]Cl_2$ (**1**), $[(BimH)_3Ni^{II}(L_1)(L_2)][NO_3]_2$ (**2**), and $[(BimH)_3Ni^{II}(\kappa^2O_2NO)](NO_3)$ (**3**). These complexes are characterized by different methods such as ^1H, ESI-MS, SCXRD, UV-Vis, FT-IR. **2** and **3** are used to synthesis a main precursor $[(BimH)_3Ni^{II}(\kappa^2\text{-}ONO)][NO_3]$ (**4**) complex. Acid induced reduction of **4** leads to detachment of nitrite from the nickel sites as evident from the disappearance of the nitrite band in the FTIR. ESI-MS spectra reveals the formation of 3,5-di-tert-butylcatechol which is an indirect evidence of the homolytic N-O bond cleavage upon protonation.

Table of content

Introduction

In 1992, nitric oxide (NO) was crowned the "Molecule of the Year" by Science magazine, coinciding with the publication of the research article "NO News Is Good News".[1] This article asserted that "A startlingly simple molecule unites neuroscience, physiology, and immunology and revises scientists' understanding of how cells communicate and defend themselves."[1]

NO plays a pivotal role in sustaining life on earth. It facilitates vasodilation and regulates neurotransmission, immune response, platelet aggregation, apoptosis, and gene expression. Additionally, NO serves as a mediator for a wide range of both antitumor and antimicrobial activities.[2,3] NO generation in mammals occur through two pathways: the two-step oxidation of L-arginine to NO and citrulline by nitric oxide synthases or utilizing nitrite as a biological reservoir for NO production via nitrite reductases.[4]

In recent times, various types of model complexes related to nitric oxide generation have been prepared and extensively studied using different spectroscopic methods. This is important for a better understanding of the metal active sites in proteins and provides mechanistic insight into the reaction pathway. Four major classes of reactions have been explored for NO_2^- reduction chemistry:

1) Acid induced nitrite reduction (mimicking NO_2^- reductases, NiRs): Mechanistic and theoretical studies indicate that ancillary proton delivery to the prosthetic group is a critical step to cleave N-O bond and favour the release H_2O and NO in enzymatic nitrite reduction. Different functional model complexes also follow this pathway to release NO. In the catalytic cycle, an elusive nitrous acid complex is formed and tends to cleave N-OH bond to generate the metal-nitrosyl complex which subsequently releases nitric oxide. [5,6]

2) Oxygen atom transfer (OAT) triggered by oxophilic substrate: Enzymatic studies have shown that heme proteins such as cytochrome c, with proximal S-donor ligands, are efficient catalysts for nitrite reduction through OAT reaction. This observation suggests that thioether (R_2S), thiols (RSH), Phosphines (PR_3) types oxophilic substrate can reduce the nitrite complex to metal-nitrosyl species and subsequently form sulfoxide, sulfenic acid, and phosphine oxide respectively. [7-10]

3) Phenol oxidation and NO generation (O-nitrosation and ArO-NO cleavage): Different types of phenol can be used for the formation of NO form metal-nitrite complex. In this process, phenol acts as a reductant and also proton source. Initially, metal-bound nitrous acid species are generated, followed by the production of reactive O-nitrosated intermediates called ArO-NO which readily release NO. [11]

4) Transnitrosation via nucleophilic attack at metal-nitrite: Nucleophiles with a proton source promote the formation of nitric oxide from metal-nitrite complex. In this reaction nucleophile attacks one of the N-O bond of the [M(II)](κ2-O_2N) species, resulting in the production of [M^{II}-OH] species and the nitrosated nucleophile Nu-NO (Nu =NPh_2, O^tBu, SR).[12]

Functional and structural model complexes

Karlin and co-workers synthesized a heme/copper assembly that mimics the $heme_{a3}/Cu_B$ active site of cytochrome c oxidase, enabling the interconversion of NO_2^- to NO.[13,14] Partially reduced heme/Cu assembly can reduce NO_2^-, with the heme center oxidized by one electron while copper acts as a spectator in this process. This results in the generation of a μ-oxo heme-Fe^{III}-O-Cu^{II} species which also facilitates NO oxidation to nitrite. Subsequently, a reduced heme and Cu^{II}-nitrito complex are formed.[13,14] In 1937, Brooks first investigated the NiR activity of hemoglobin and demonstrated nitric oxide generation and metHb formation in anaerobic conditions.[15] Biomimetic modeling of NiR enzyme reveals the possible structure and reactivity of the elusive intermediates during reaction but few reports on mechanistic studies of nitrite reduction which helps to create efficient catalyst for NO production and stabilizing the metal-nitrosyl complex.[6] Papish et al. used hydrotris(triazolyl)borate ligand, a good π-acceptor ligand stabilizes the unusual Cu(I) nitrite complex for the first time and acts as functional model of NiR.[16] This monoanionic Cu(I) complex allows the stoichiometric reduction of NO_2^- in presence of acid.[15] Murphy et al. isolated the metal-nitrosyl complex in enzymatic study for the first time and proved that reduction of metal-nitrite first converts to metal-nitrosyl and then releases NO.[16] Ford et al. used R_2S and tetrahydrothiophene as catalyst for nitrite reduction in Fe-porphyrin complex.[7] Harrop et al. synthesized non-heme $Fe(NO_2)_2$ complex which exhibits stoichiometric and catalytic NiR activity using thiol. This non-heme iron complex displays unique properties of selective turnover of NO_2^- into NO and is the first structurally characterized non-heme iron center with a nitrite group in trans position.[8a] Warren et

al. investigated the reactivity of a β-diketiminato copper(II) nitrito complex with thiols for NO production.[8b] In this scenario, the thiol acts as a nucleophile and attacks the copper center, leading to the formation of an S-nitrosation product, copper hydroxide, and NO.[8b] Hsu et al. used a Cu(I) nitrite complex to produce NO using two equivalents of protons and in this study, they got a crystal of nitrous acid intermediates for the first time.[18] Patra et al. studied Cu(II)- nitrite complex for generation of NO using acetic acid and an electrochemical technique was used to detect and quantify NO.[19] Hunt et al. employed electrolytic method for reduction of NO_2^- at copper center.[20b] Lenhert et al. developed a copper(II) complex based catalyst which is O_2 tolerant can reduce nitrite electrochemically at the optimal potential.[21] Pankaj et al. explored the cobalt-nitrite complex for its reduction using acid. This study found that upon protonation of the nitrite complex, it generates NO and H_2O_2 through $\{CoII\text{-}NO\}^8$ intermediates. This group also used non-heme iron $[(12TMC)Fe^{II}(NO_2^-)]^+$ complex to investigate the acid induce formation of NO. This metal-nitrite complex transforms into $\{FeNO\}^7$ species in the reaction medium.[22,23]

In recent times, there has been increased attention on utilizing acid-induced nitrite reduction to create efficient and low-cost catalysts for NO generation. Different by-product formations are possible in this process, so more mechanistic and theoretical studies are needed to understand the basis for formation of these side-products. Very few metal-nitrite complexes are reported for nitrite reduction in the presence of acid, so we focus on these pathways for NO generation.[5,6]

Yunho Lee and coworkers designed a PNP nickel scaffold (PNP=$N[2\text{-}p^ipr_2\text{-}4\text{-}Me\text{-}C_6H_3]_2$) which acts as a universal platform for the deoxygenation of NO_x substrate.[24] In this event carbon monoxide accept the oxygen atom from nitrite and nitrate to form CO_2 and driving force of the reaction.[24] For the first time nitrate to dinitrogen formation is possible using this nickel complex.[24] This finding influences us to used nickel metal for nitrite reduction and nickel(I) complexes are known for small molecule activation such as N_2O, O_2, S_8, P_4.[24]We report the formation of a nickel-nitrite complex using the known $(BimH)_3$ ligand. To date, there is no knowledge of nitrite reduction mediated by a Ni metal center and redox-inactive ligand framework, although many copper and iron-bound nitrite complexes are reported for NO generation. To generate this Ni-nitrite complex we design different paths to get desired product. We synthesized main precursor $[(BimH)_3Ni^{II}(\kappa^2\text{-}ONO)][NO_3]$ complex for nitrite reduction in two different

paths. To reduce nitrite, we used triflic acid (1equiv.) and 2,4-di-tert-butylphenol (2.5 equiv.) which acts as radical quencher. UV-vis, FTIR, ESI-MS were used for monitoring the reaction and characterized the possible end products.

Results and Discussion:

Synthesis and characterization of complexes:

The $(BimH)_3$ ligand was synthesized following a procedure that has been reported previously.[26,27] Metalation of $(BimH)_3$ with $NiCl_2.6H_2O$ in methanol produces a dark-greenish complex, $[(BimH)_3Ni^{II}(\mu\text{-}Cl)_2Ni^{II}(BimH)_3]Cl_2$ (**1**) (Scheme 1). The progress of the reaction was monitored using UV-vis spectroscopy (Figure 1).

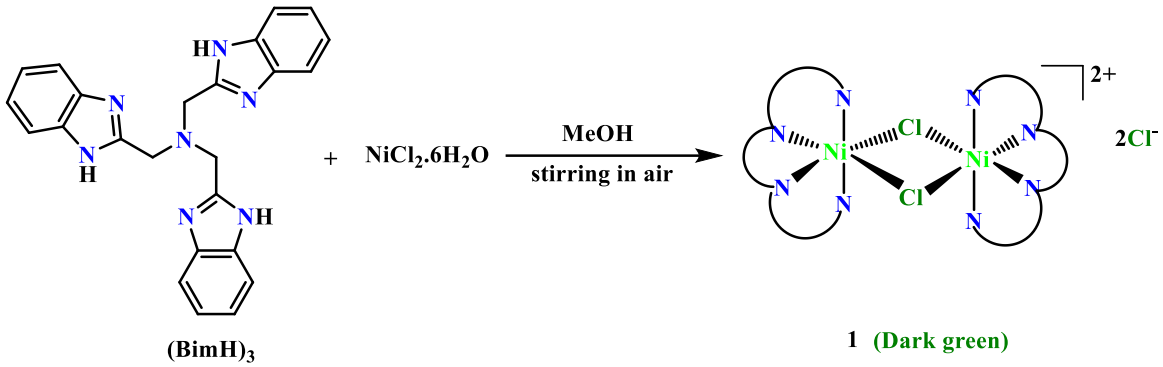

Scheme 1: Synthesis of $[(BimH)_3Ni^{II}(\mu\text{-}Cl)_2Ni^{II}(BimH)_3]Cl_2$ complex (**1**)

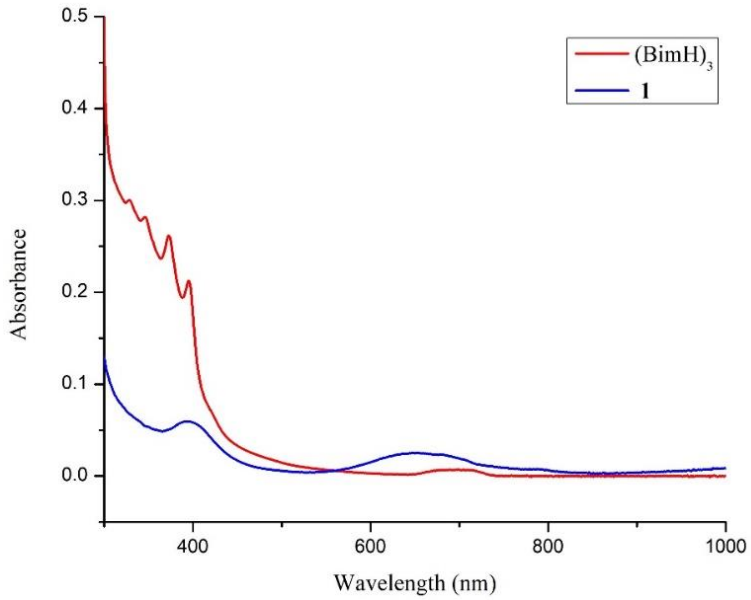

Figure 1: The UV-visible absorption spectra of **1** and $(BimH)_3$ ligand recorded in DMF at room temperature.

The UV-visible spectrum of **1** in DMF gives rise to two distinct broad absorbances around 650 nm and 400 nm which originates from metal centers d-d transition and ligand centered π – π* transitions, respectively.[28]

The molecular structure of **1** was confirmed by single crystal X-ray diffraction (Figure 2). Slow evaporation of dark greenish methanolic solution of **1** at room temperature resulted in green blocked shaped crystal within 3-4 days. In this complex, two nickel centres are bridged by two chloride atoms, and each metal center is coordinated to the $(BimH)_3$ ligand in tetradentate fashion. Both Ni centers in **1** display a distorted octahedral geometry. The other two chloride ions in second coordination sphere, balance the overall charge of the complex. The bond distances between the Ni and coordinated nitrogen atoms of benzimidazole moieties (2.026(6) - 2.031(6) Å) are relatively shorter than the Ni-N1 (tertiary amine) bond length (2.193(6) Å). This creates flexibility within the molecule. Selected bond distances (Å) and bond angles (°) and crystallographic parameters are listed in Tables 1 and S1, respectively.

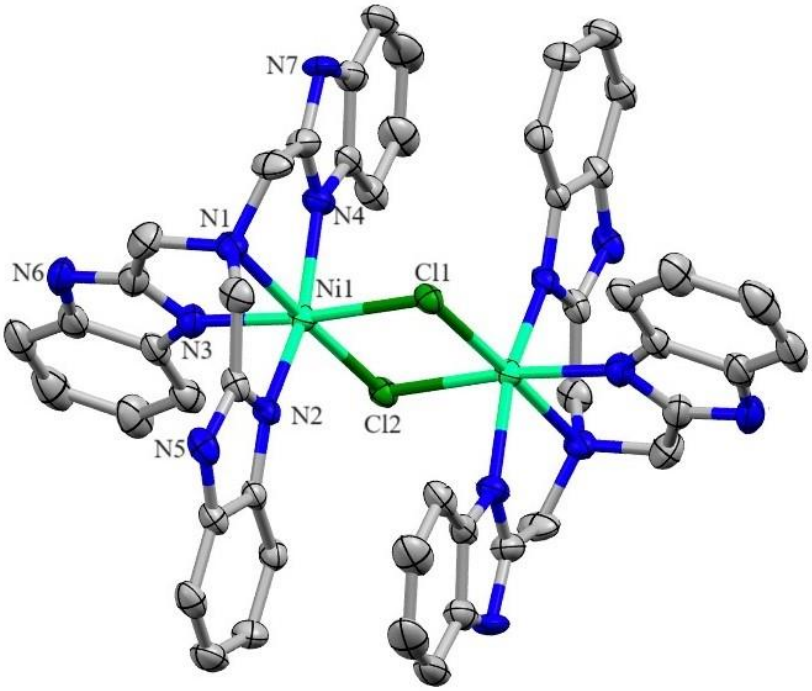

Figure 2: Molecular structure of **1** in the solid state (thermal ellipsoids at 30%, H atoms and counter anions omitted for clarity).

Table 1: Selected bond distances [Å] and bond angles [°] of **1**

Bond distances [Å]	
Ni1-N1	2.193(6)
Ni1-N2	2.026(6)
Ni1-N3	2.031(6)
Ni1-N4	2.024(6)
Ni1-Cl1	2.496(2)
Ni1-Cl2	2.354(2)
Bond angles [°]	
Cl1-Ni1-Cl2	89.26(6)
Cl2-Ni1-N3	99.26(2)
N3-Ni1-N1	82.54(2)
N1-Ni1-Cl1	88.93(2)
Cl1-Ni1-N3	171.38(2)
N4-Ni1-N2	159.12(2)
N4-Ni1-Cl2	100.21(2)
N4-Ni1-N3	88.71(2)
N4-Ni1-N1	78.92(2)
Cl2-Ni1-N1	178.01(2)
N3-Ni1-N2	90.75(2)
N4-Ni1-Cl1	88.48(2)

The presence of fully occupied coordination sites around the Ni centres in **1** prevents substrate binding. To address this, a 1:1 CH_3OH:CH_3CN solution of **1** was treated with 4 equivalents of silver nitrate which resulted in an immediate color change from dark green to deep blue and eventually a blue precipitate was obtained (Scheme 2). The resulting product is a mixture of two monomeric Ni complexes, **2a** and **2b**, as revealed by the x-ray structure of the complexes (vide infra).

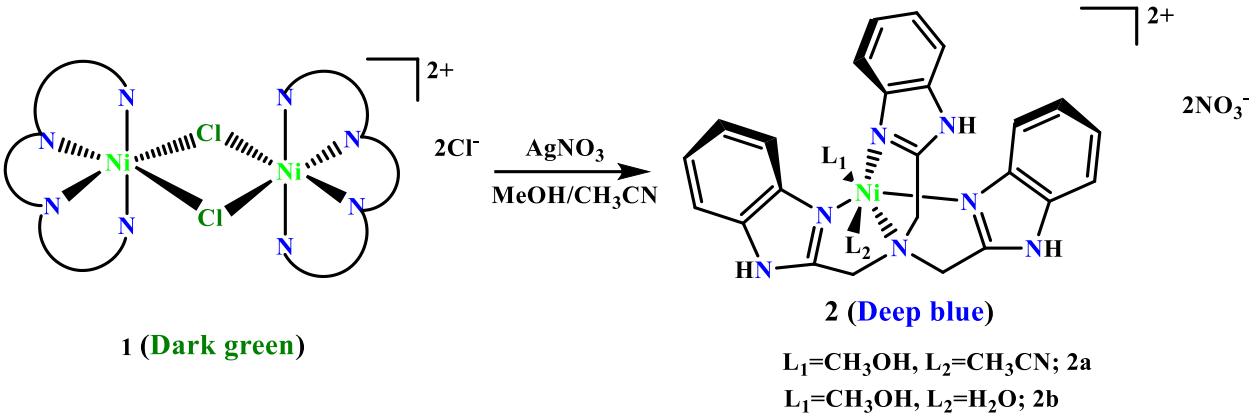

Scheme 2: Synthesis of $[(BimH)_3Ni^{II}(L_1)(L_2)][NO_3]_2$complex (**2)**

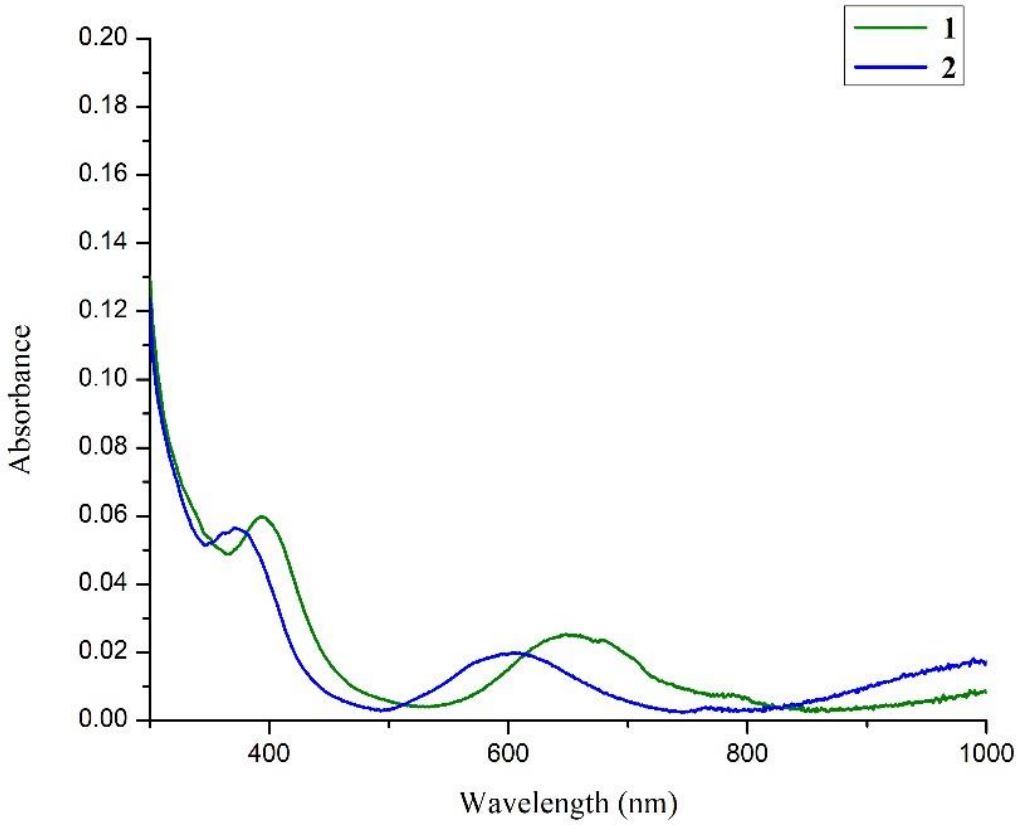

Figure 3: The UV-visible absorption spectra of **1** and **2** recorded in DMF at room temperature.

The UV-visible spectrum of **2** (Figure 3) is different from **1** and both bands that are present in **1** are shifted towards lower wavelength (blue shift). **2** in DMF solvent gives a characteristic broadband at 600 nm region which is responsible for the d-d transition of Ni(II) and ligand centered π – π* transitions are responsible for 380 nm peak. The electrospray ionization mass spectra of **2** in positive mode shows that two free N-H

bond of imidazole ring heterolytically cleaved and balance the charge of nickel, resulting in a neutral complex. This neutral compound is ionized by H^+ and gives 464.1135 peak. ESI-MS spectra of (**2**) given below in figure 4:

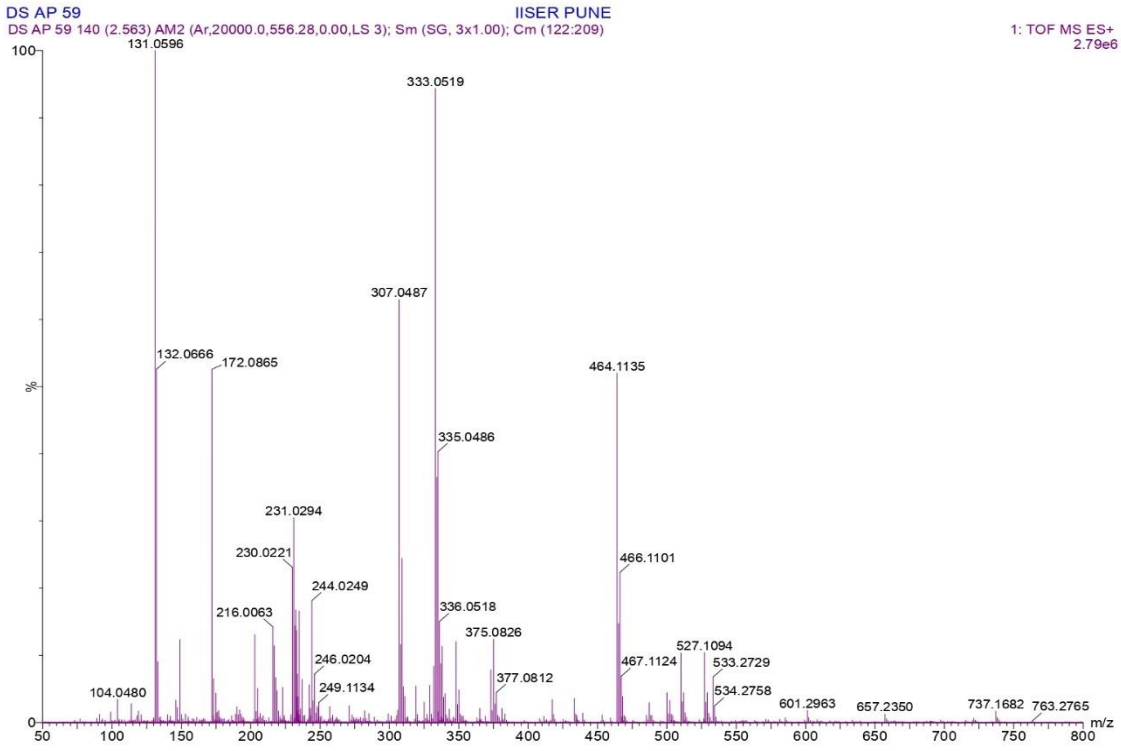

Figure 4: ESI-MS spectra (positive mode) of **2**

Dissolving **2** in a mixture of acetonitrile-methanol and allowing it to slowly evaporate at room temperature resulted in the formation of blue-colored crystals after a few days. Two independent molecules are present in the asymmetric unit: one with coordinated acetonitrile and methanol solvent molecules **2a**, and the other with coordinated methanol and water **2b** (Figure 5). The remaining coordination sites for both molecules are occupied by tetradentate $(BimH)_3$ ligand and two nitrate anions in the second coordination sphere balance the overall charge for both complexes. Trans angles measurements indicate that the geometry around the metal is distorted octahedral in both complexes. The selected structural parameters and crystallographic data are given in table 2 and table S2, respectively.

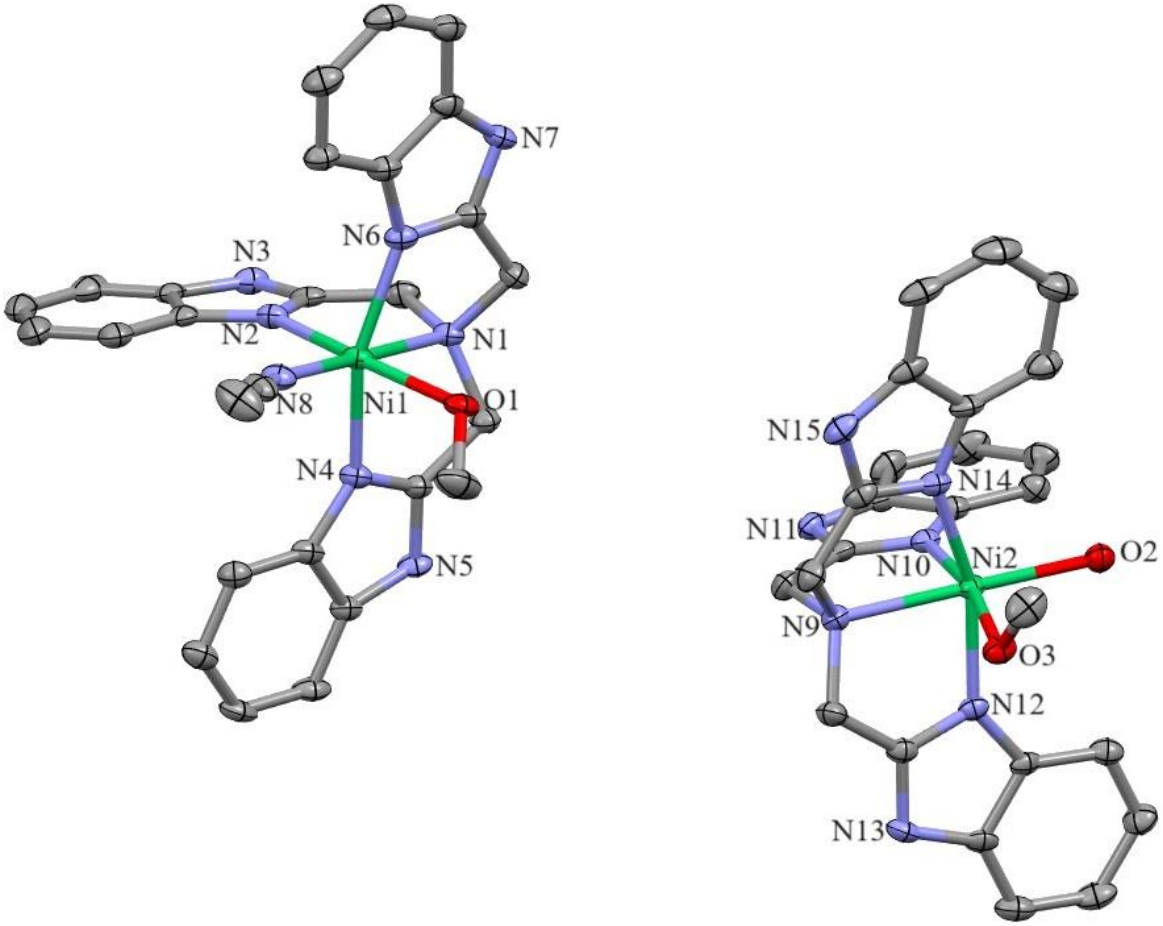

Figure 5: Molecular structure of **2a** and **2b** in the solid state (thermal ellipsoids at 30%, H atoms and counter anions omitted for clarity)

Table 2: Selected bond distances [Å] and bond angles [°] of **2a** and **2b**

Bond distances [Å]	
Ni1-N1	2.190(3)
Ni1-N2	2.045(3)
Ni1-N4	2.040(3)
Ni1-N6	2.062(3)
Ni1-O1	2.126(3)
Ni1-N8	2.053(3)
Ni2-N9	2.193(3)
Ni2-N10	2.077(3)
Ni2-N12	2.022(3)
Ni2-N14	2.022(3)
Ni2-O2	2.047(2)
Ni2-O3	2.151(2)
Bond angles [°]	
N1-Ni1-N8	176.02(1)
N2-Ni1-O1	169.77(1)
N4-Ni1-N6	159.17(1)
N1-Ni1-N4	80.70(1)
N4-Ni1-N8	101.55(1)
N8-Ni1-N6	97.46(1)
N6-Ni1-N1	79.85(1)
O1-Ni1-N1	88.75(1)
O1-Ni1-N8	88.32(1)
N2-Ni1-N1	81.78(1)
N9-Ni2-O2	174.36(1)
N10-Ni2-O3	169.59(1)
N12-Ni2-N14	159.51(1)
O2-Ni2-N10	103.60(1)

N10-Ni2-N9	81.67(1)
N9-Ni2-O3	88.95(1)
O2-Ni2-O3	85.95(1)
N9-Ni2-N12	81.39(1)
N9-Ni2-N14	80.47(1)
O2-Ni2-N12	100.32(1)

Alternatively, when the free $(BimH)_3$ ligand was treated with nickel nitrate hexahydrate in methanol, a blue coloured complex, $[(BimH)_3Ni^{II}(\kappa^2\text{-}O_2NO)][NO_3]$ (**3**), was obtained (Scheme 3).

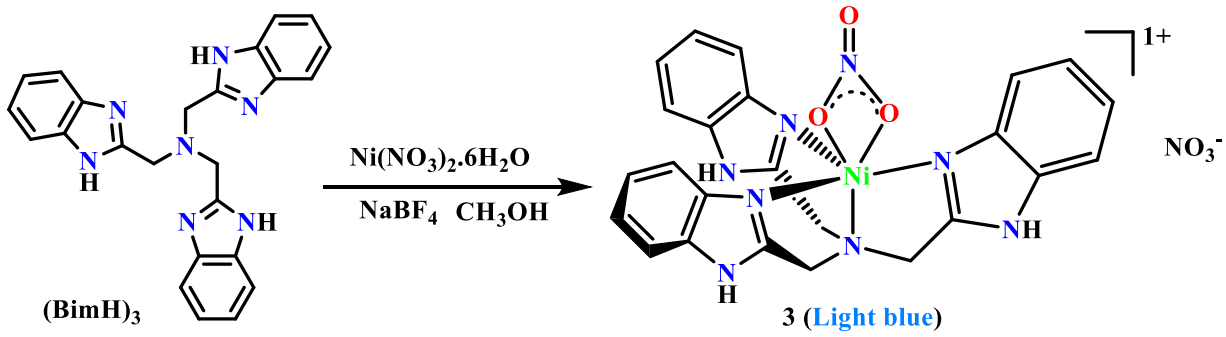

Scheme 3: Synthesis of $[(BimH)_3Ni^{II}(\kappa^2\text{-}O_2NO)][NO_3]$ complex (**3**)

The progress of the reaction was monitored using UV-vis spectroscopy (Figure 6). The UV-Visible spectrum of **3** in DMF gives rise to two distinct broad absorbances around 600 nm and 380 nm which originates from metal centers d-d transition and ligand centered π – π* transitions, respectively. [28]

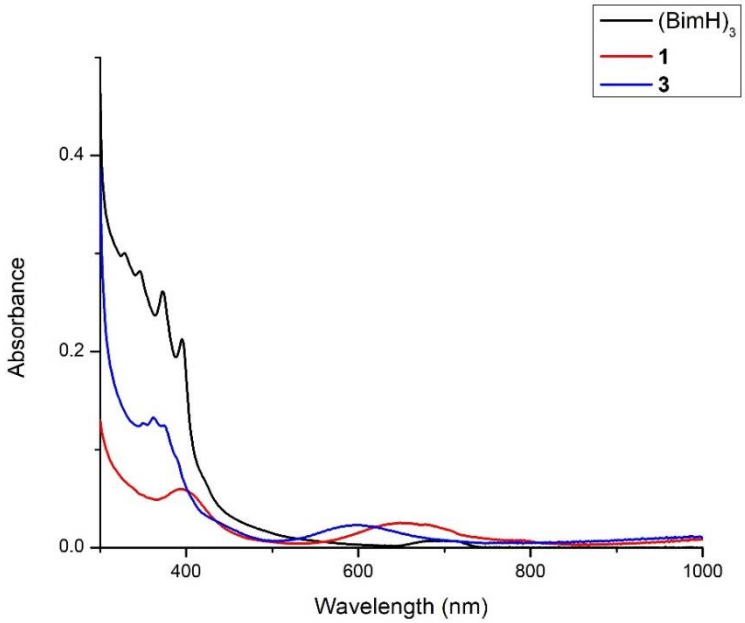

Figure 6: The UV-visible absorption spectra of **(BimH)$_3$**, **1,** and **3** recorded in DMF at room temperature.

Reactivity Studies of the Ni-Bim complexes

Complexes **2** and **3** upon treatment with 1.3 equivalent of sodium nitrite resulted in the formation of the desired nitrite bound metal complex [(BimH)$_3$Ni^{II}(κ^2-ONO)][NO$_3$] (**4)** (Scheme 4). The color of the reaction mixture turned pale blue immediately after addition of sodium nitrite followed by the formation of a pale blue solid product, **4**.

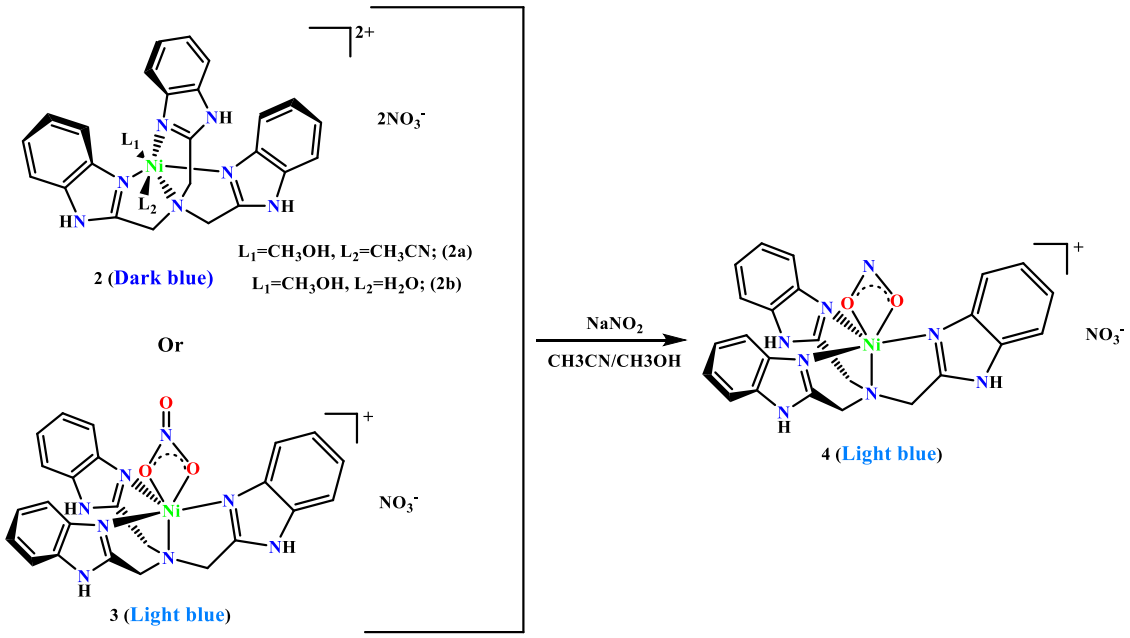

Scheme 4: Synthesis of complex **4**

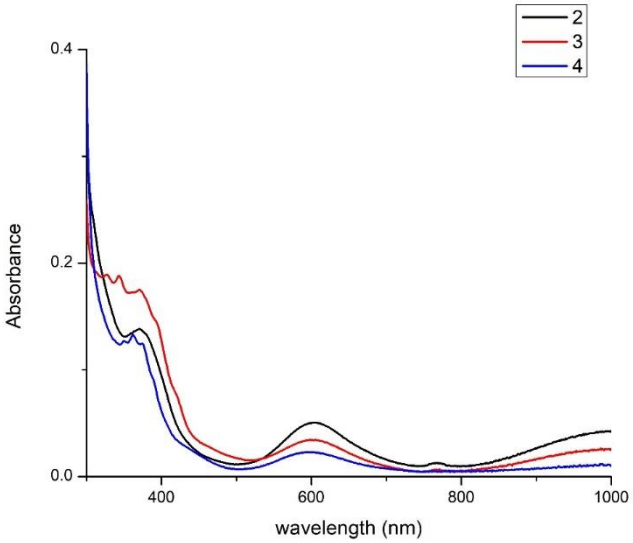

Figure 7: The UV-visible absorption spectra of **2**, **3**and **4** recorded in DMF at room temperature.

Figure 7 shows the UV-vis spectrum of complexes **2**, **3**, and **4**. **4** exhibits a broad band at lower energy region (1000 nm) which is absent in solvent coordinated complexes and other two peaks shift towards higher wavelength (red shift) with respect to **2** and **3**. A new band arises at 1278.78 cm^{-1} in FT-IR spectrum of **4** (Figure 8) but this band is absent in **2** which indicates nitrite binding to metal center.

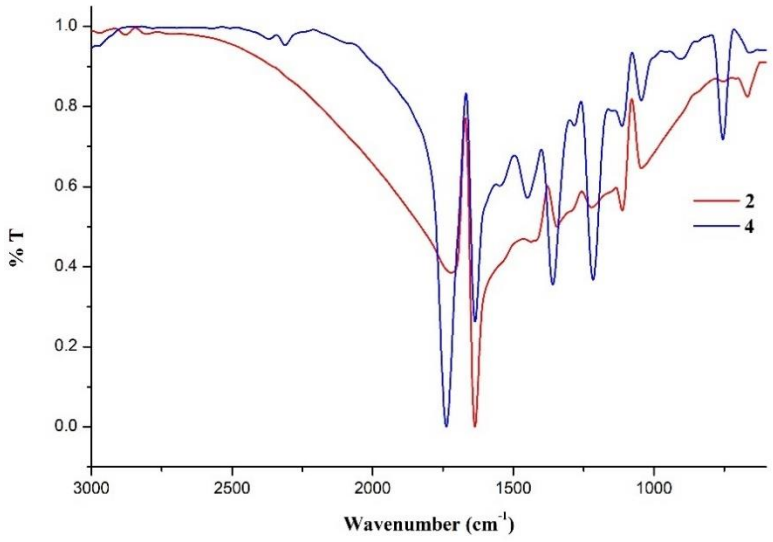

Figure 8: FTIR (KBr) spectra of **2** and **4**

X-ray quality single crystals of **4** was obtained by the slow evaporation of a methanol-acetonitrile (1:1) solution at room temperature. Crystal structure of **4** (Figure 9) reveals that nitrite binds the metal center in a bidentate fashion and four nitrogen atoms of the

$(BimH)_3$ ligand coordinates to the metal centre resulting in a distorted octahedral geometry. Both N8-O1 and N8-O2 bond lengths of the nitrite is very similar which indicates the delocalization of the negative charge. The selected structural parameters and crystallographic data are given in tables 3 and S3.

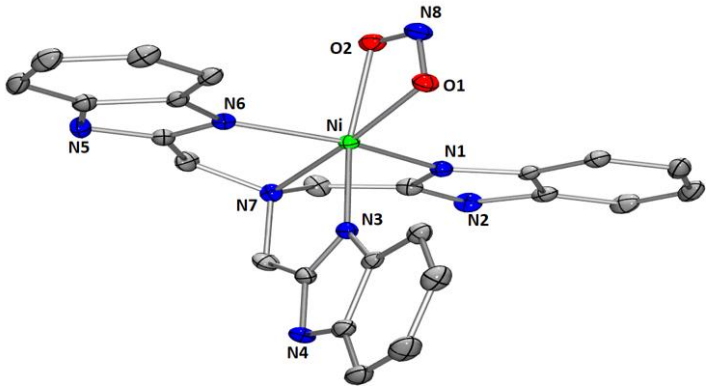

Figure 9: Molecular structure of **4** in the solid state (thermal ellipsoids at 30%, H atoms and counter anion omitted for clarity)

Table – 3 Selected bond distances [Å] and bond angles [°]

Bond distances [Å]	
Ni-O1	2.061(3)
Ni-O2	2.129(3)
O1-N8	1.263(6)
O2-N8	1.259(6)
N7-Ni	2.208(3)
N3-Ni	1.987(3)
N1-Ni	2.047(4)
N6-Ni	2.049(4)
Bonds Angles [°]	
O1-N8-O2	112.15(1)
O1-Ni-O2	59.90(1)
N7-Ni-N1	79.53(1)
N7-Ni-N6	79.20(1)

N3-Ni-N7	82.86(1)
N3-Ni-N1	94.09(1)
N3-Ni-N6	90.74(1)
N6-Ni-N1	157.41(1)

Nitrite reductase activity of complex 4

To investigate the nitrite reductase activity of **4**, we tested the reactivity of the complex towards acids such as, acetic acid and triflic acid, which is the first step towards the reduction of nitrite to NO. In metal-nitrite complexes, the acids are known to protonate the nitrite resulting an elusive $\{LM(ONOH)\}^{2+}$ species which has the tendency to break one N-O bond homolytically resulting in the formation of highly reactive hydroxyl radical and NO. The resulting hydroxyl radical can be indirectly detected by the use of a radical quencher, 2,4 di-tert-butyl phenol.[5,6]

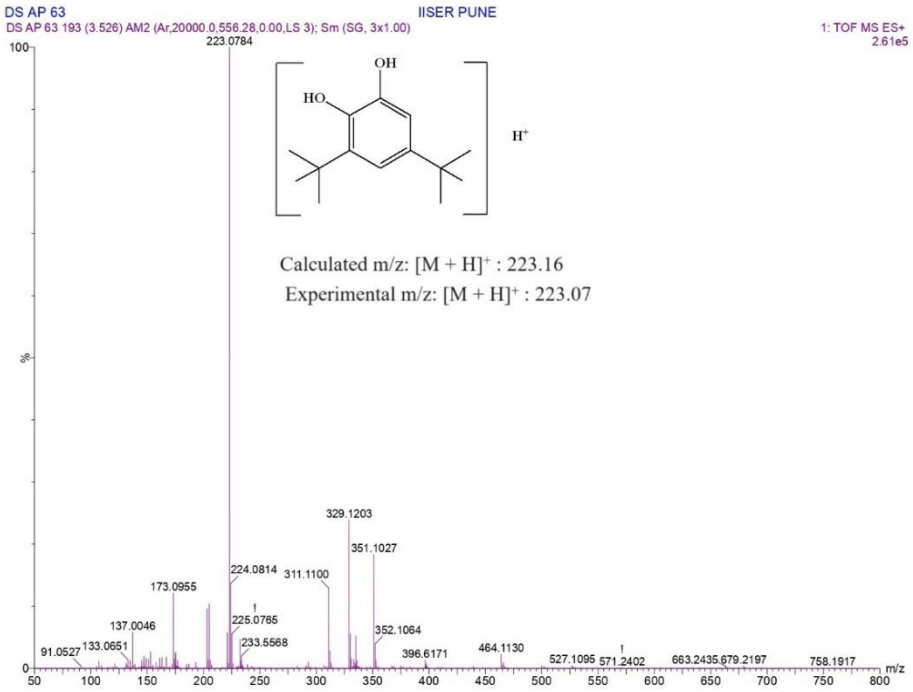

Figure 10: ESI-MS data to detect possible side products

We attempted to identify the products of the reaction using ESI-MS technique (Figure 10). We detected a peak corresponding to 3,5-di-tert-butyl catechol at $[M + H]^+$:

223.0784. A second signal at 464.1130 corresponds to nitrite free metal complex, similar to that observed in the ESI-MS spectra of **2**, was also observed. Together this suggests that the bound nitrite has detach from metal sites upon treatment with acid and results in the conversion of 2,4-di-tert-butylphenol to 3,5-di-tert-butylcatechol. Scheme 5 shows the proposed reaction pathway based on our experimental observations.

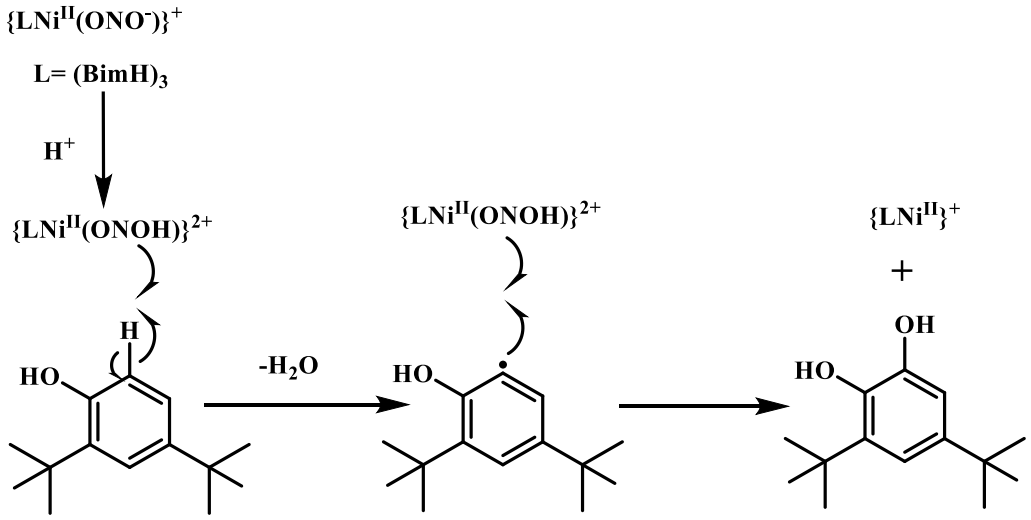

Scheme 5: Possible reaction pathway for nitrite reduction.[5,6]

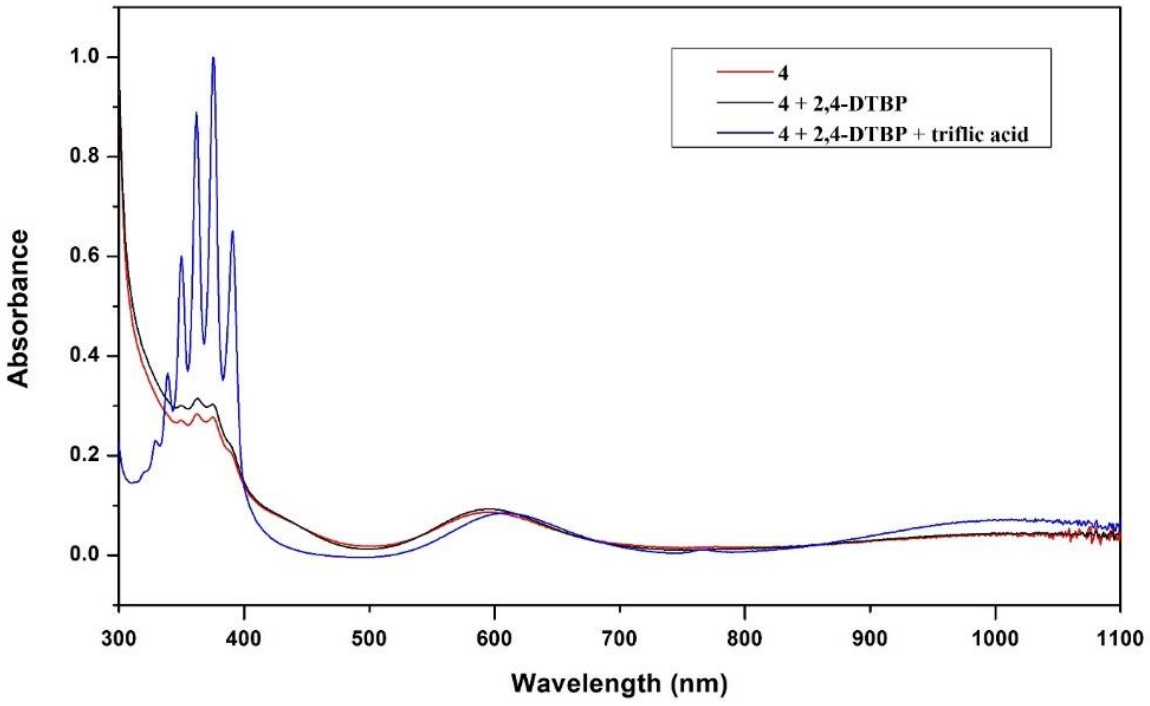

Figure 11: Electronic absorption spectra of **4** (red line) and **4** + phenol + triflic acid (blue line).

The reaction was monitored by UV-vis spectroscopy (Figure 11) which indicates the band shift and new band generation due to new species production and FTIR spectra indicate that after the addition of acid characteristic NO_2^- band disappeared and resembled to **2**. (Figure 12).

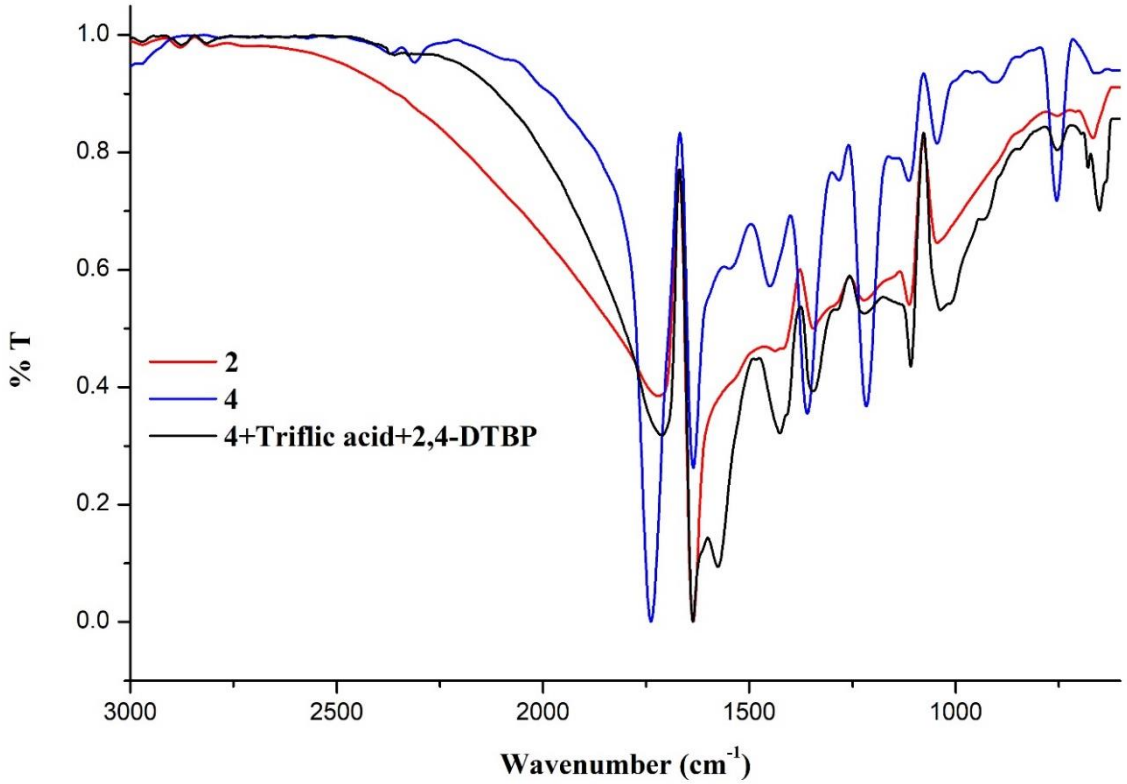

Figure 12: FTIR (KBr) spectra of **2**, **4,** and **4**+triflic acid+2,4-DTBP

Summary and future directions

In this study we report the synthesis, structural and spectroscopic characterization of nickel complexes and their reactivity towards nitrite reduction. To make metal complexes we used $(BimH)_3$ ligand. Metallation of $(BimH)_3$ with $NiCl_2$ yielded $[(BimH)_3Ni^{II}(\mu\text{-}Cl)_2Ni^{II}(BimH)_3]Cl_2$ (**1**) which is coordinatively saturated. Reaction of **1** with silver nitrite generates $[(BimH)_3Ni^{II}(L_1)(L_2)][NO_3]_2$ (**2**) with solvent coordinated sites that are more accessible towards substrate binding. The nitrate-bound nickel complex $[(BimH)_3Ni^{II}(\kappa^2\text{-}O_2NO)][NO_3]$ (**3**) was synthesized by treatment of **2** with nickel nitrate. In the next step, complex **2** and **3** further undergoes ligand metathesis with sodium nitrite to obtain the nitrite-bound complex $[(BimH)_3Ni^{II}(\kappa^2\text{-}ONO)][NO_3]$ (**4**). All complexes were characterized by different spectroscopic techniques such as ^1H, ESI-MS, UV, FT-IR, SCXRD. **4** upon treatment with acid undergoes changes in the UV-vis and FTIR spectra indicating the absence of nitrite in the product complex. When this reaction was performed in presence of 2,4-di-tert-butylphenol, a radical trap, it leads to the formation of 3,5-di-tert-butylcatechol as evidenced in the ESI-MS spectrum of the product. This suggests a homolytic cleavage of the N-O bond of the nitrite during the reaction. Further studies are needed to prove and quantify nitric oxide formation to support our proposed mechanism.

Materials and Methods

General procedures

All reagents and solvents were purchased from commercial suppliers (Avra, Srl, Finar, Alfa Aesar) and used without further purification unless otherwise noted. ^{1}H, ^{13}C spectra were obtained at 298 K using ARX 400 (^{1}H, 400MHz; ^{13}C, 100.46 MHz) spectrometers from the Bruker. Chemical shifts are reported as δ (ppm) values, using either TMS or residual solvent peaks as an internal standard and coupling constants (J) as Hz values. The short notations for the multiplicity of the signals are as follows: br = broad, m = multiplet, s = singlet, d = doublet, t = triplet, q = quartet, and sept = septet. High-resolution mass spectra were obtained using WATERS G2 Synapt Mass Spectrometer. The presentation of the mass spectra is in the standard form, m/z. UV-Vis spectra were recorded using a Agilent Cary 60 spectrophotometer at room temperature. The wavelength was recorded from 1000-300 nm at a scan speed of 400 nm/min and a data interval of 1 nm. Solutions for UV–vis analyses were prepared freshly by dissolving isolated compounds in anhydrous solvents unless otherwise mentioned. FTIR spectra (with 4 cm^{-1} spectral resolution) were collected on a Shimadzu IRPrestige–21 FTIR spectrometer. Solid samples were mixed with KBr (FTIR grade) for preparing pellets.

Crystallographic Details

Single crystals of all complexes were mounted under mineral oil on a glass capillary. Data for all compounds were collected at 296 K, 273 K on a Bruker Kappa diffractometer equipped with an APEXII CCD detector and Mo fine focus sealed tube source. All the data were collected by employing graphite monochromated MoKα radiation (λ = 0.7107 Å) and the data sets were processed using APEX IV software. Integration of the data sets were carried out with the Bruker SAINT program. Structure solutions were performed using SHELXTS1 and refined employing SHELXLS1 through OLEX2S2 program. Intensities were corrected for Lorentz and polarization effects and an empirical absorption correction was applied using Blessing's method as incorporated into the program SADABS.S3. Non-hydrogen atoms were refined with anisotropic thermal parameters. The positions of the hydrogen atoms were calculated

in the idealized positions unless otherwise noted. The molecular structures were rendered using MERCURY 3.10.3 software.

Synthesis of $(BimH)_3$ ligand

Tris((1H-benzo[d]imidazol-2-yl)methyl)amine, $(BimH)_3$, ligand was synthesized and characterized according to the previously reported procedure.[10,11] In a 100-mL flask, trinitriloacetic acid (1.5 g, 20 mmol), o-phenylenediamine (6g, 30 mmol) and 20 ml of ethylene glycol were added and the mixture was heated at 200^0C for 24 hours. After cooling, the product was precipitated in 100 ml of ice-cooled water. The solid was filtered, washed with 150 ml of cool water, and further purified by recrystallization process using ethanol to afford the pure product as a white powder. Yield = 1.2 g (65%).

^{1}H NMR (400 MHz, CD_3OD): δ 6.92-6.85 (m, 6H), 6.60-6.53 (m, 6H), 2.97-2.92 (s, 6H)

MS (ESI) m/z: $[M + H]^+$ = 408.1928 (Obs.), 408.1920 (Calc.).

FT-IR Cm^{-1}: 1273 {v (C-N)}, 1437 {v (C=N)}

Synthesis of $[(BimH)_3Ni^{II}(\mu\text{-}Cl)_2Ni^{II}(BimH)_3]Cl_2$ (1)

Nickel(II) chloride hexahydrate (87.945 mg, 0.370 mmol) dissolved in methanol (5 ml) was added dropwise to a methanol suspension (20 ml) of $(BimH)_3$ (150.8 mg, 0.370 mmol) with stirring in air. During the reaction, the mixture formed a clear greenish solution. Stirring was continued for 4 hours, and the solution was filtered, and then fully dried under vacuum. The solid product was dissolved in methanol-dichloromethane solvent mixture (3:1) to get the crystal of this product. Yield = 450 mg (78%)

UV-Vis in DMF: 400 nm, 650nm(broad) peak.

Single crystal XRD data confirms the formation of this complex and due to solubility issues, we could not perform other spectroscopic analysis for further characterization of this complex.

Synthesis of $[(BimH)_3Ni^{II}(L_1)(L_2)][NO_3]_2$ complex (2)

Silver nitrate dissolved in methanol (5ml) was added dropwise to the metal complex (**1**) solution in acetonitrile-methanol solvent mixture. The reaction mixture was stirred for 4 hours in air. After a few minutes, the greenish solution turned into dark blue colour. Then solvent was dried under high vacuum and got solid product. This solid was dissolved in acetonitrile-methanol solvent mixture and left it for few days. After slow evaporation, we got cube-shaped crystal of these complexes. Yield = 220 mg, (55%)

^{1}H NMR (400 MHz, DMSO-d6) δ 6.92-6.85 (m, 6H), 6.60-6.53 (m, 6H), 2.97-2.92 (s, 6H)

MS (ESI) m/z: $[M + H]^+$: 464.1134 (Obs.), 464.1030 (Calc.)

UV-vis: 380 nm, 600 nm.

FT-IR Cm^{-1}: 1273 {v (C-N)}, 1437 cm^{-1}{v (C=N)}

Synthesis of $[(BimH)_3Ni^{II}(\kappa^2\text{-}O_2NO)][NO_3]$ complex (3)

Nickel(II) nitrate hexahydrate (186.978 mg, 0.643 mmol) dissolved in methanol (10ml) was added to the sodium tetrafluoroborate (142.8 mg, 0.643 mmol) solution (10ml) to get nickel(II) tetrafluoroborate hexahydrate metal salt. The reaction mixture was stirred for 12 hours in air. No observable colour change was noticed during the reaction. After 12 hours, $(BimH)_3$ ligand (262 mg, 0.643 mmol) solution in methanol (15 ml) was added to the metal salt solution and again stirred for 4 hours. A bluish-white coloured solution formed rapidly. After completion of this reaction, solvent was dried under high vacuum to get solid product. Then solid product was dissolved in acetonitrile-methanol solvent mixture and left it for 2 days. Due to slow evaporation, we got blue coloured cube-shaped crystal of this complex.

UV-Vis: 375 nm, 600 nm.

Synthesis of $[(BimH)_3Ni(\kappa^2\text{-}ONO)][NO_3]$ (4)

In this step, we used complex (2a and 2b) as a starting reagent dissolved in the methanol-acetonitrile solvent mixture. Then excess sodium nitrite solution in methanol

(5 ml) was added to the complex (2a and2b) solution. The reaction was stirred for two hours in air at room temperature. After adding sodium nitrite, colour change was observed immediately from dark blue to green. After that, the solution was filtered and dried under high vacuum. Acetonitrile-methanol solvent mixture was used to dissolve solid product. This solution was placed in a 100 ml conical and left it for few days. Crystal of this complex was observed when most of the solvent was evaporated.

^{1}H NMR (400 MHz, DMSO-d6) δ 6.92-6.85 (m, 6H), 6.60-6.53 (m, 6H), 2.97-2.92 (s, 6H)

MS (ESI) m/z: $[M + H]^+$: 510.12 (Obs.), 510.10 (calc.)

UV-vis: 600nm, 385nm

FT-IR (Cm^{-1}): 1278.78{v (O-N-O)}

Reactions of Nickel(II)-nitrite Complex (4) with triflic acid

First $[(BimH)_3Ni(\kappa^2\text{-}ONO)][NO_3]$ complex (0.102 mg, 0.178 mmol) was dissolved in acetonitrile- methanol solvent mixture, and after few minutes 2,4-di-tertbutyl phenol (91.81 mg, 0.445 mmol) in methanol solvent (5 ml) was added to the metal complex solution. After that 1 equivalent w.r.t complex (**4**) triflic acid transfer to the reaction mixture and immediately dark blue colour of the solution was transformed into sky blue. The reaction was stirred at room temperature for two hours. Then solvent was dried under high vavuum and got solid product.

MS (ESI) m/z: $[M + H]^+$: 223.07(2.4-DTBP), 464.11($2 + H^+$)

UV-vis: 1007,607, 390, 375, 361, 348, 338, 328 nm

FT-IR Cm^{-1}: 1742, 1649, 1362, 1212.

References

1) Koshland, D. E., Jr. *Science* **1992**, *258*, 1861-1861.

2) a) Furchgott, R. F. *Angew. Chem. Int. Ed*. **1999**, *38*, 1870–1880; b) Ignarro, L. J. *Angew. Chem. Int. Ed*. **1999**, *38*, 1882–1892; c) Ignarro, L. J. *Biology and Pathobiology*, Academic press, **2000**; d) Lehnert, N.; Kim, E.; Dong, H. T.; Harland, J. B.; Hunt, A. P.; Manickas, E. C.; Oakley, K. M.; Pham, J.; Reed, G. C.; Alfaro, V. S. *Chem. Rev*. **2021**, *121*, 14682–14905.

3) Maia, L. B.; Moura, J. J. G. *Chem. Rev.* **2014**, *114*, 5273-5357.

4) Hunt, A. P.; Lehnert, N. *Acc. Chem. Res*. **2015**, *48*, 2117−2125.

5) Kulbir; Das, S.; Devi, T.; Ghosh, S.; Sahoo, S. C.; Kumar, P. *Chem. Sci*. **2023**, *14*, 2935–2942.

6) Bhardwaj, P.; Kulbir; Devi, T.; Kumar, P. *Inorg. Chem. Front*, **2023**, *10*, 7285.

7) Kurtikyan, T. S.; Hovhannisyan, A. A.; Iretskii, A. V.; Ford, P. C. *Inorg. Chem.* **2009**, *48*, 11236-11241.

8) a) Sanders, B. C.; Hassan, S. M.; Harrop, T. C. *J. Am. Chem. Soc.*, **2014**, *136*, 10230–10233; b) Kundu, S.; Kim, W. Y.; Bertke, J. A.; Warren, T. H. *J. Am. Chem. Soc.*, **2017**, *139*, 1045–1048.

9) a) Patra, A. K.; Afsher, R. K.; Rowland, J. M.; Olmstead, M. M.; Mascharak, P. K. *Angew. Chem., Int. Ed*., **2003***, 42*, 4517–4521; b) Cheng, L.; Powell, D. R.; Khan, M. A.; Richter-Addo, G. B. *Chem. Commun.,* **2000**, 2301-2302.

10) Sahana, T.; Valappil, A. K.; Amma, A. S. P. R.; Kundu, S. *ACS Org. Inorg. Au* **2023**, *3*, 246-253.

11) Anju, B. S.; Nair, N. R.; Kundu, S. *Angew. Chem., Int. Ed*., **2023**, *62*, e202311523.

12) Kundu, S.; Kim, W. Y.; Bertke, J. A.; Warren, T. H. *J. Am. Chem. Soc*. **2017**, *139*, 1045- 1048.

13) Hematian, S.; Sieglar, M. A.; Karlin, K. D. *J. Am. Chem. Soc.* **2012**, *134*, 18912–18915.

14) Hematian, S.; Kenkel, I.; Shubina, T. E.; Dürr, M.; Liu, J. J.; Siegler, M. A.; Ivanovic-Burmazovic, I.;Karlin, K. D. *J. Am. Chem. Soc.* **2015**, *137*, 6602–6615.

15) Brooks, J.; Keilin, D. *Proc. R. Soc. London, Ser. B.***1937**, *123*, 368–382.

16) Kumar, M.; Dixon, N. A.; Merkle, A. C.; Zeller. M.; Lehnert, N.; Papish, E. T. *Inorg. Chem.*, **2012**, *51*, 7004– 7006.

17) Tocheva, E. I.; Rosell, F. I.; Mauk, A.G.; and M. E. Murphy, M.E. *Science*, **2004**, *304*, 867–870.

18) Hsu, S. C.; Chang, Y. L.; Chuang, W. J.; Chen, H. Y.; Lin, I. J.; Chiang, M. Y.; Kao, C. L.; Chen, H. Y. *Inorg. Chem*., **2012**, *51*, 9297–9308.

19) Maji, R. C.; Barman, S. K.; Roy, S.; Chatterjee, S. K.; Bowles, F. L.; Olmstead, M. M.; Patra, A. K. *Inorg. Chem*., **2013**, *52*, 11084–11095.

20) a) Speelman, A. L.; Zhang, B.; Krebs, C.; Lehnert, N. *Angew. Chem., Int. Ed*., **2016**, *55*, 6685–6688. b) Hunt, A. P.; Lehnert, N. *Acc. Chem. Res.*, **2015**, *48*, 2117–2125.

21) White, C. J.; Schwartz, J. M.; Lehnert, N.; Meyerhoff, M. E. *Bioelectrochemistry*, **2023**, 108448.

22) Puthiyaveetil Yoosaf, M. A.; Ghosh, S.; Narayan, Y.; Yadav, M.; Sahoo, S. C.; Kumar, P. *Dalton Trans*., **2019**, *48*, 13916–13920.

23) Kulbir; Das, S.; Devi, T.; Goswami, M.; Yenuganti, M.; Bhardwaj, P.; Ghosh, S.; Sahoo, S. C.; Kumar, P. *Chem. Sci*., **2021**, *12*, 10605-10612.

24) Gwak, J.; Ahn, S.; Baik, M-H.; Lee, Y. *Chem. Sci*., **2019**, *10*, 4767–4774.

25) Yao, S.; Driess, M. *Acc. Chem. Res.* **2012**, *45*, 276-287.

26)Thompson, L. K.; Ramaswamy, B. S.; Seymour, E. A *Can. J. Chem.* **1977**, *55*, 878. (b) Oki, A. R.; Bommarreddy, P. K.; Zhang, H. M.; Hosmane, N. *Inorg. Chim. Acta.* **1995**, *231*, 109.

27) Su, C.-Y.; Kang, B.-S.; Liu, Du. C.-X.; H.-Q.; Wang, Q.-G.; Mak, T. C. W. *Inorg. Chem.* **2000**, *39*, 4843-4849.

28) Wang, J.-W.; Huang, H.-H; Sun, J.-K.; Zhong, D.-C. *Acs. Catal*. **2018**, *8*, 7612-7620.

Appendix

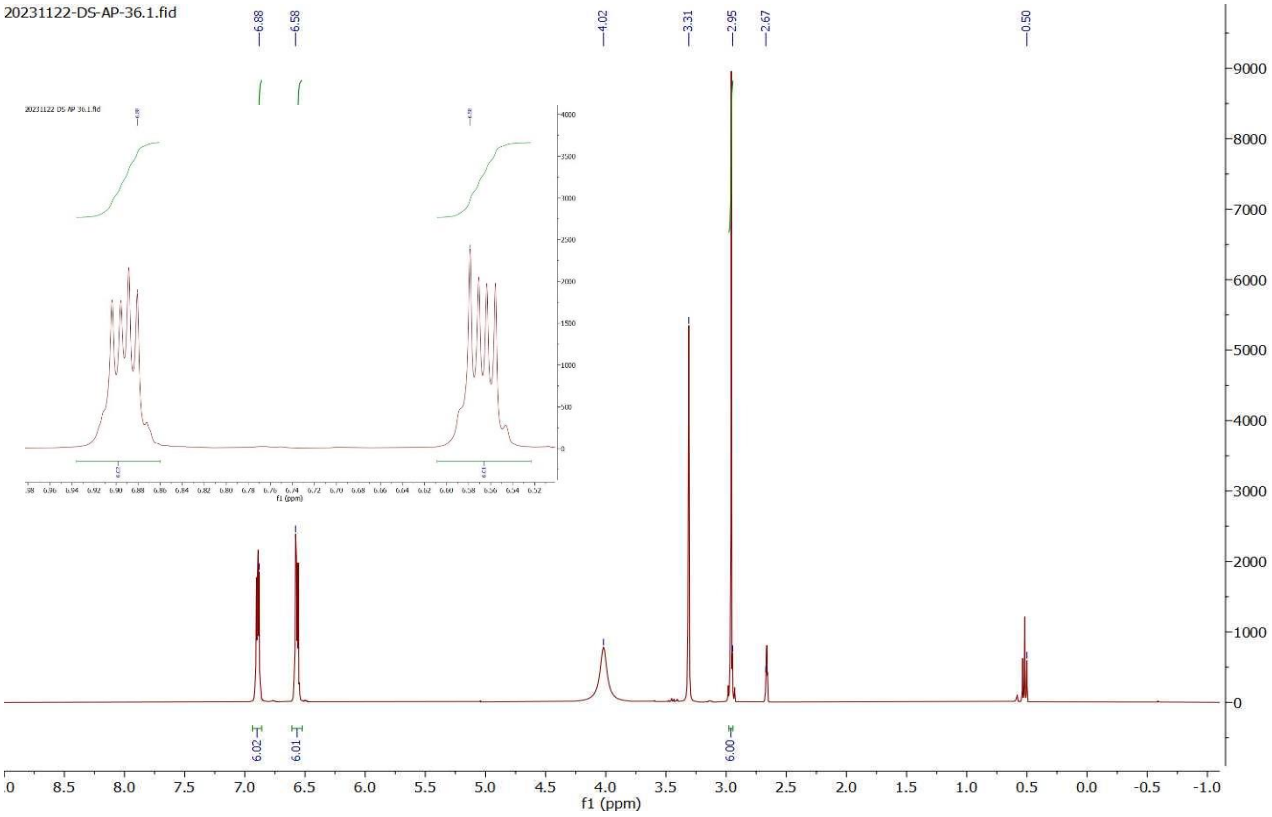

Figure S1: ^{1}H NMR spectrum (400 MHz, CD_3OD, 298K) of $(BimH)_3$ ligand

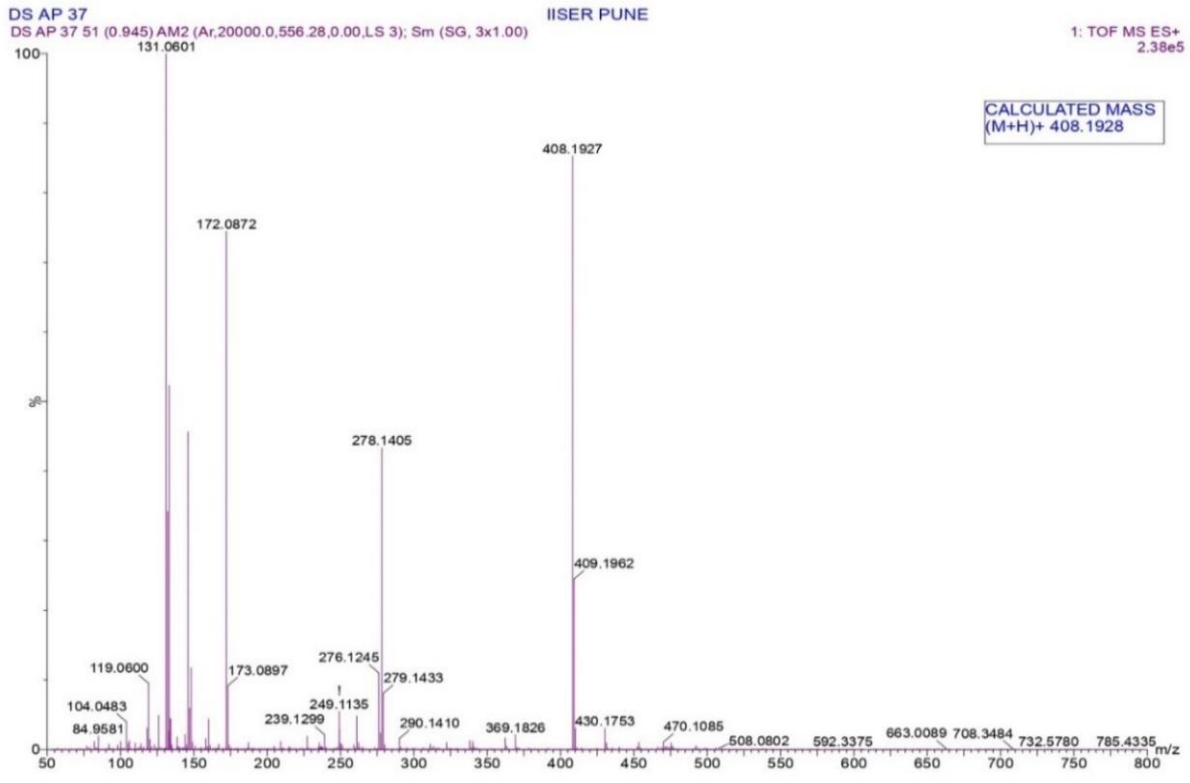

Figure S2: ESI-MS spectrum of $(BimH)_3$ ligand

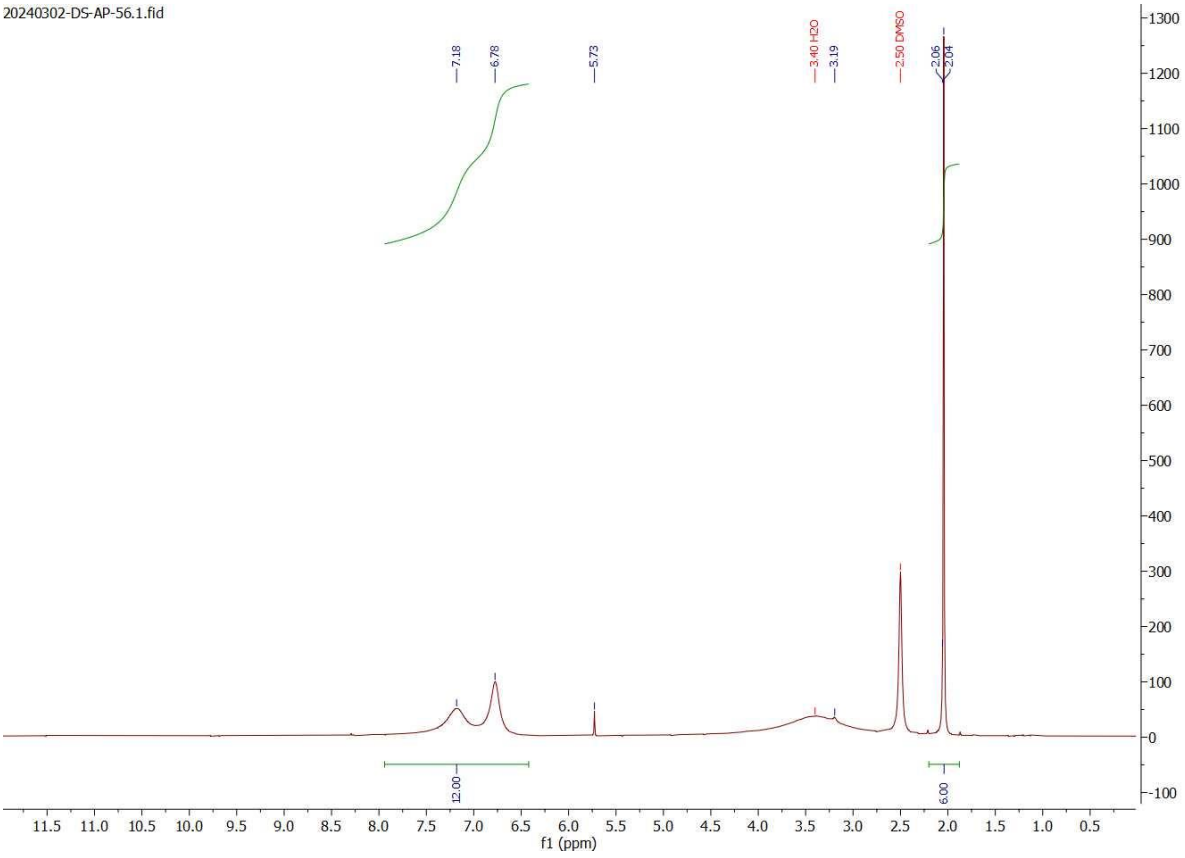

Figure S3: ^{1}H NMR spectrum (400 MHz, DMSO-d_6, 298K) of $[(BimH)_3Ni^{II}(L_1)(L_2)][NO_3]_2$

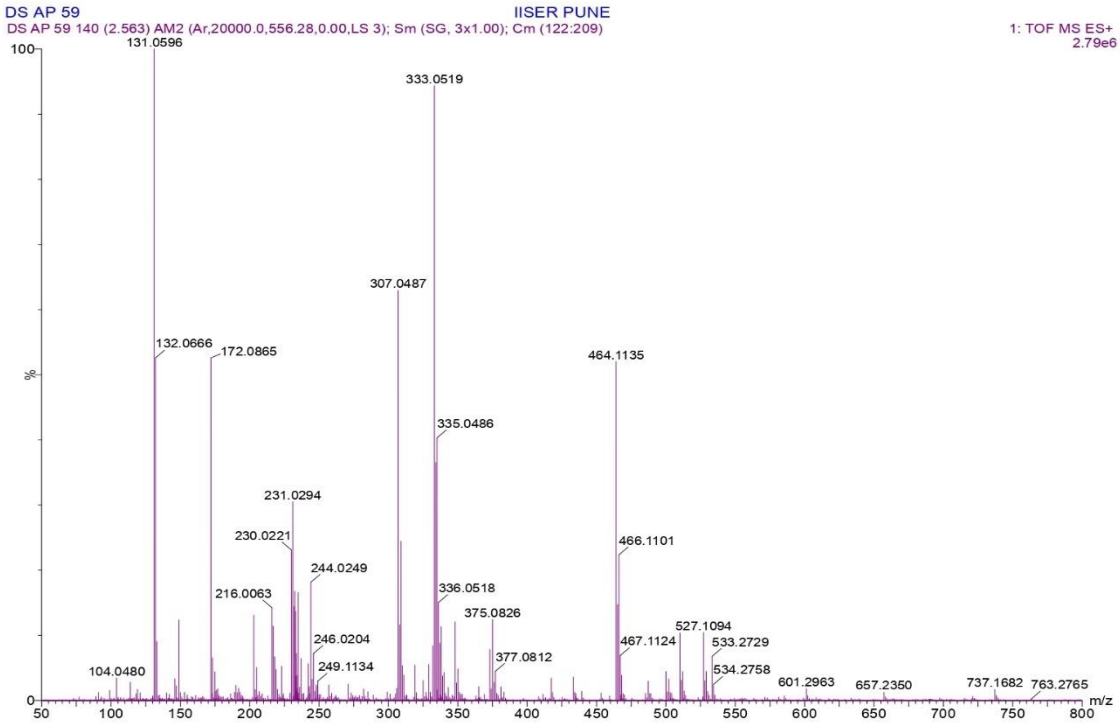

Figure S4: ESI-MS spectrum of $[(BimH)_3Ni^{II}(L_1)(L_2)][NO_3]_2$

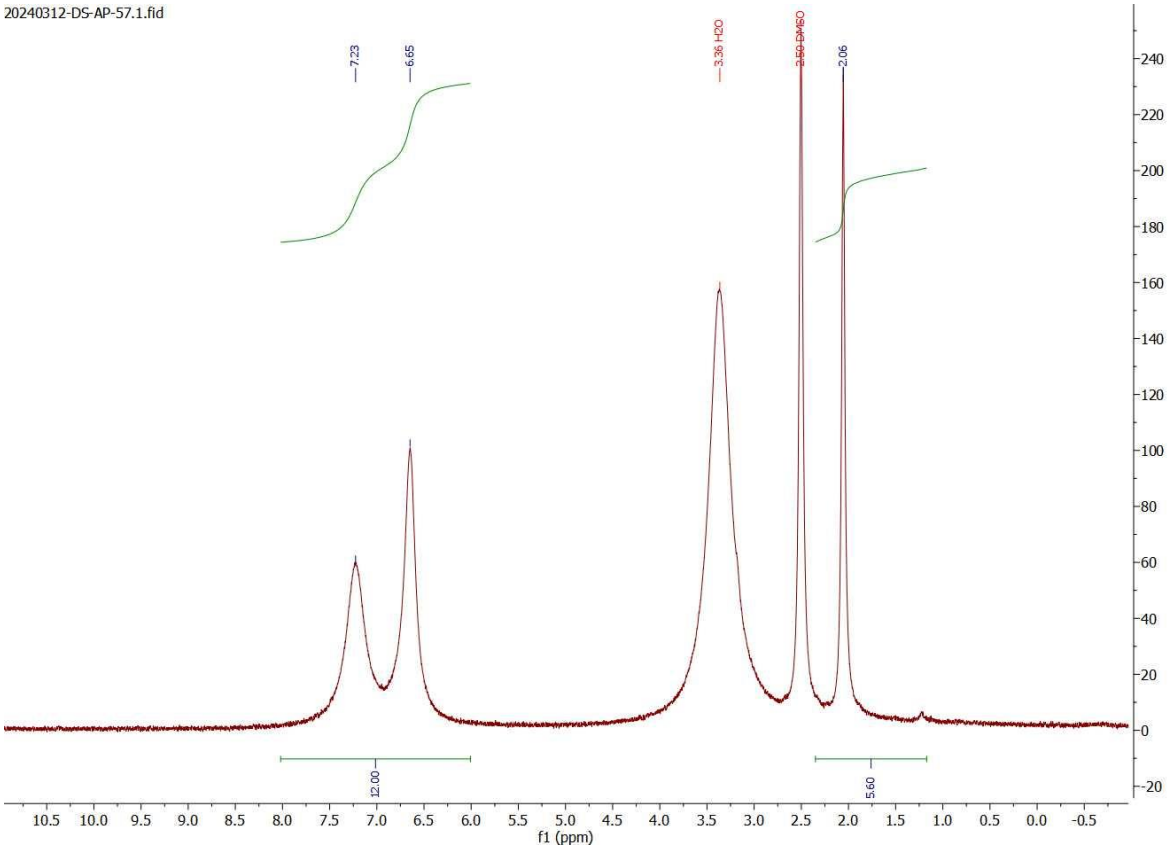

Figure S5: ^{1}H NMR spectrum (400 MHz, DMSO-d_6, 298K) of $[(BimH)_3Ni^{II}(\kappa^2\text{-}O_2NO)][NO_3]$

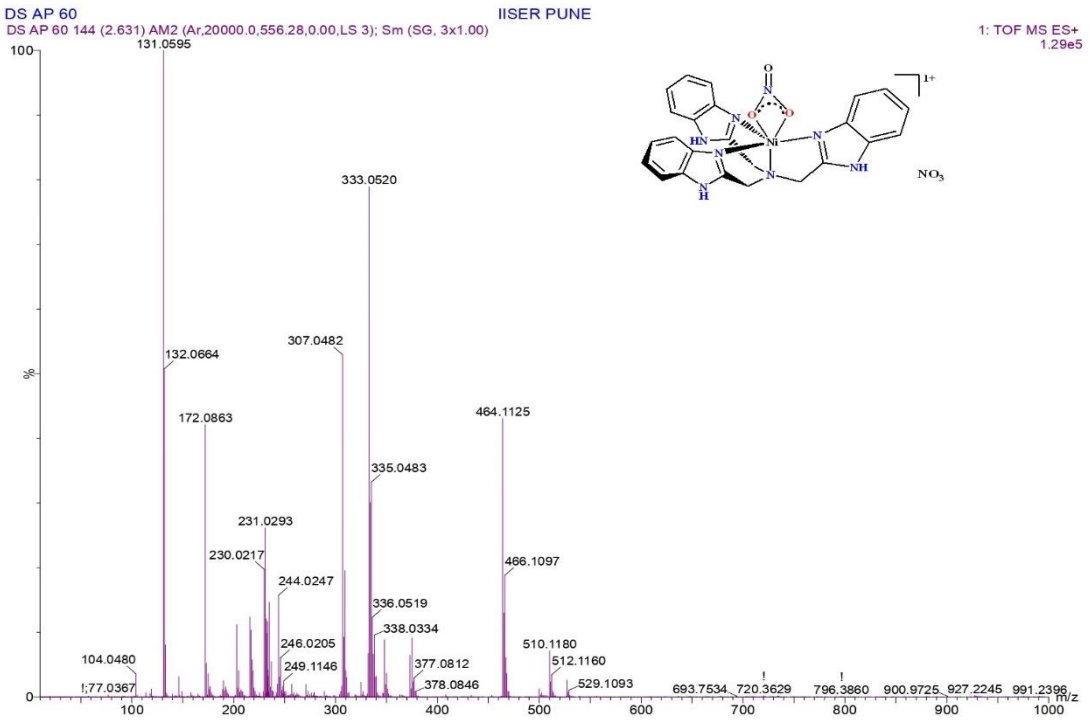

Figure S6: ESI-MS spectrum of $[(BimH)_3Ni^{II}(\kappa^2\text{-}O_2NO)][NO_3]$

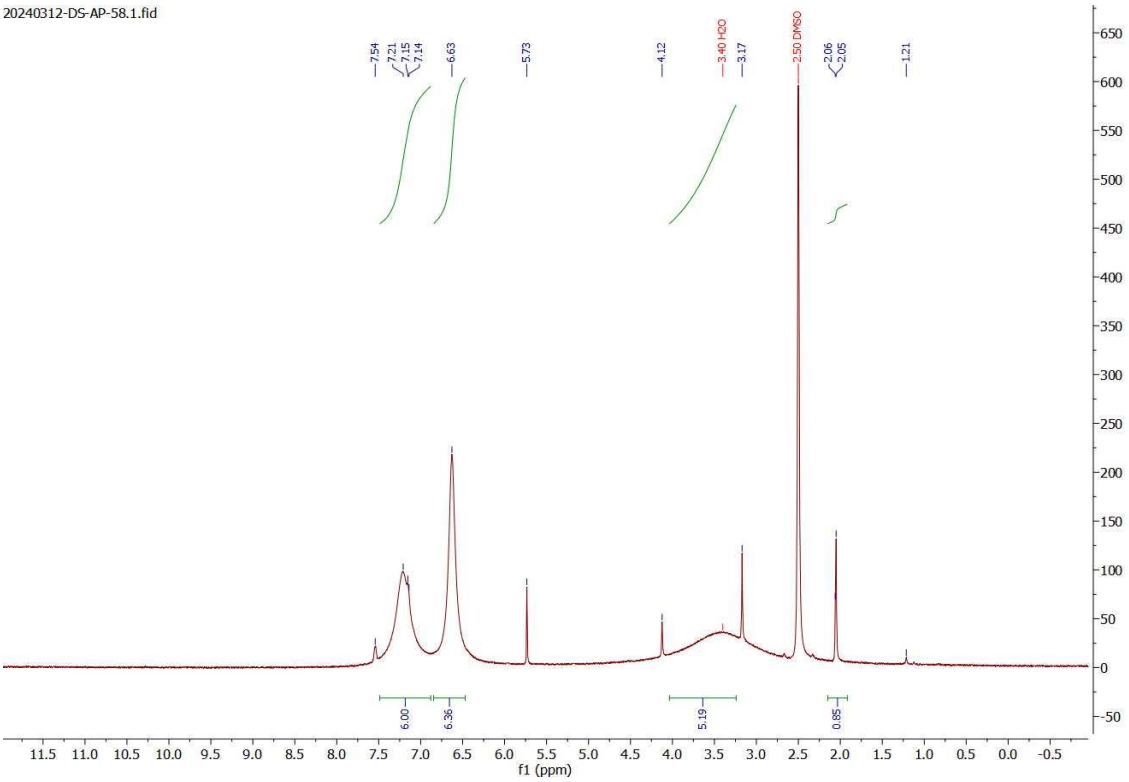

Figure S7: ^{1}H NMR spectrum (400 MHz, DMSO-d_6, 298K) of [$(BimH)_3Ni(\kappa^2$-ONO)][NO_3]

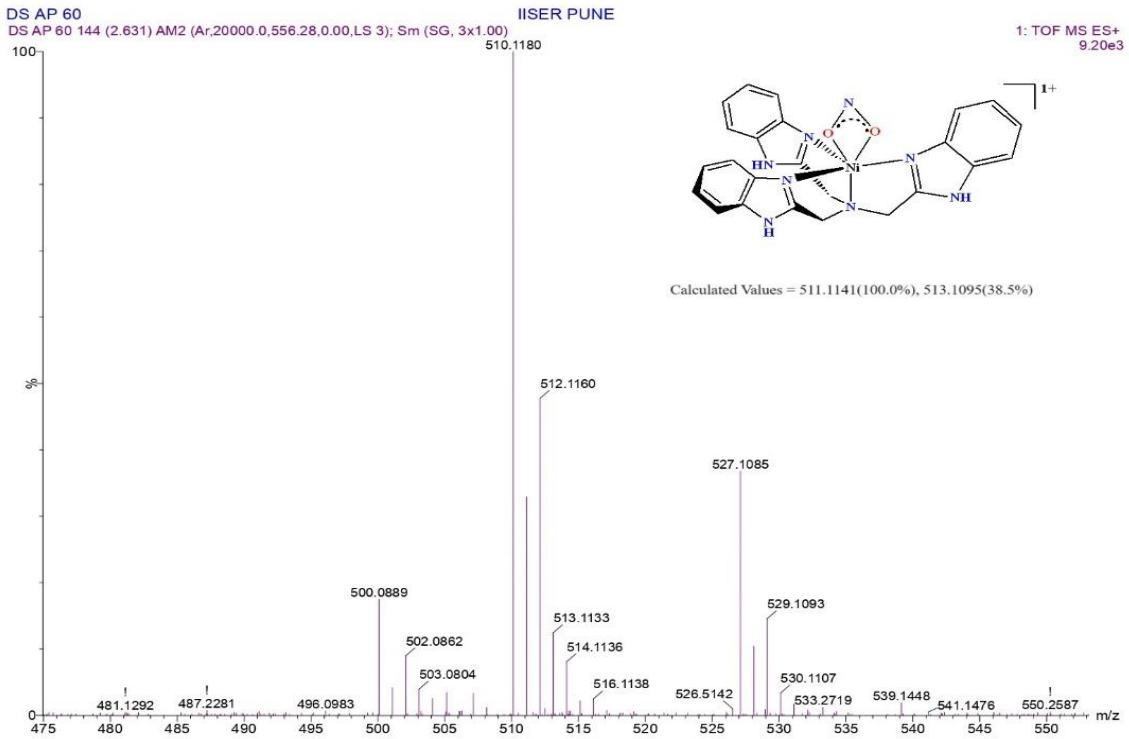

Figure S8: ESI-MS spectrum of [$(BimH)_3Ni(\kappa^2$-ONO)][NO_3]

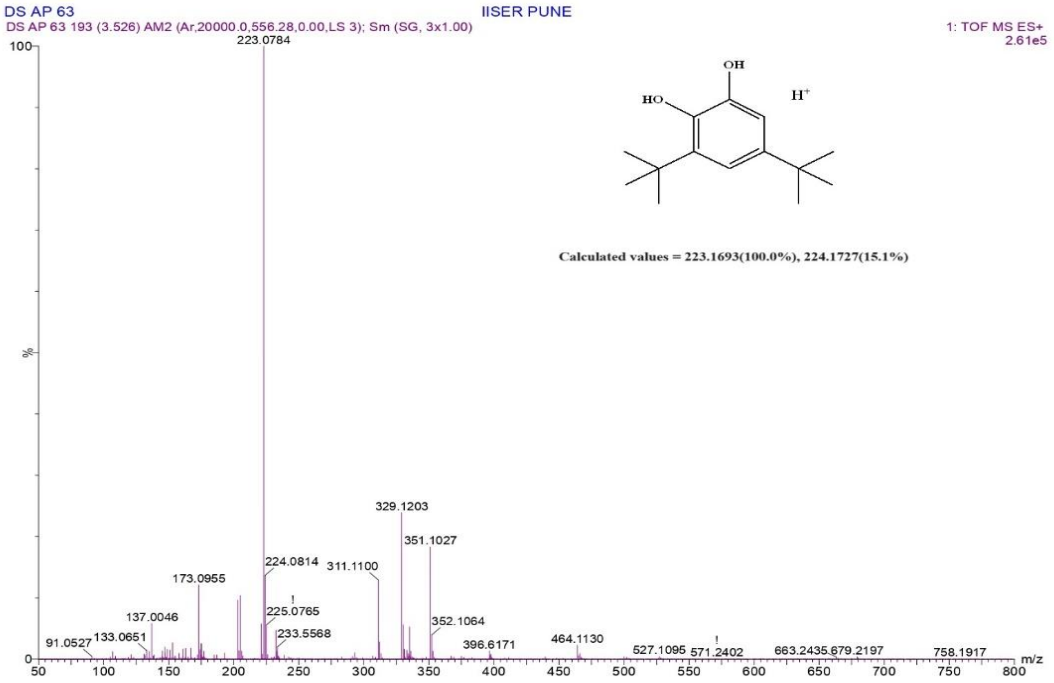

Figure S9: ESI-MS spectrum of 3,5-di-tertbutyl catechol

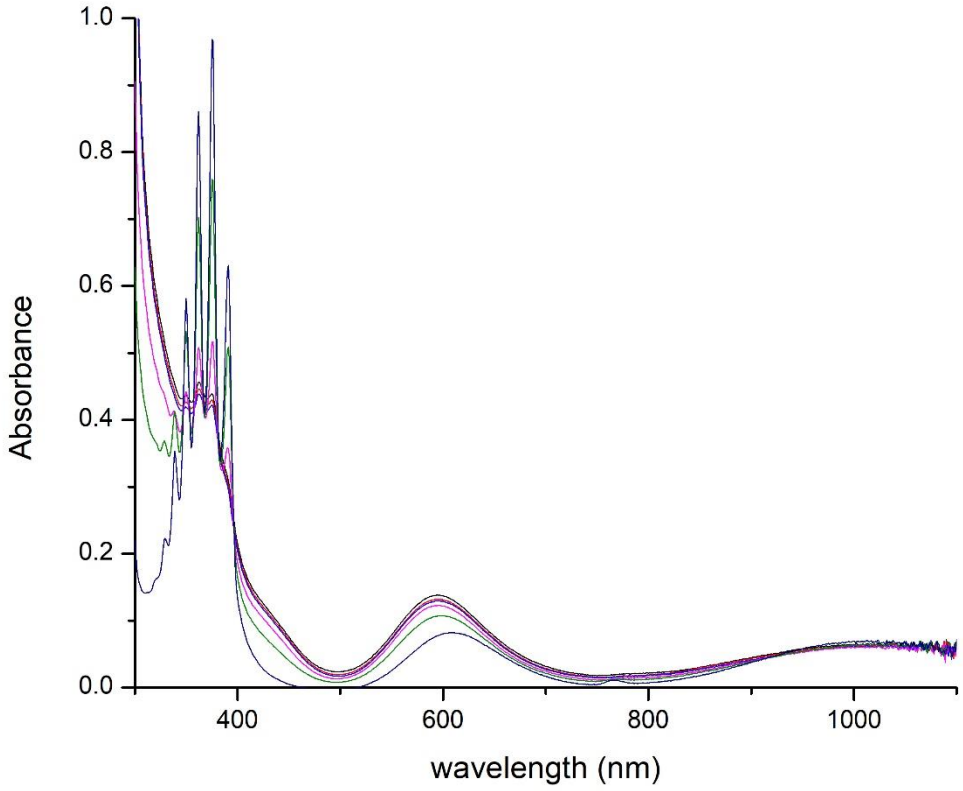

Figure S10: Qualitative titration curve of metal-nitrite, phenol, and acid

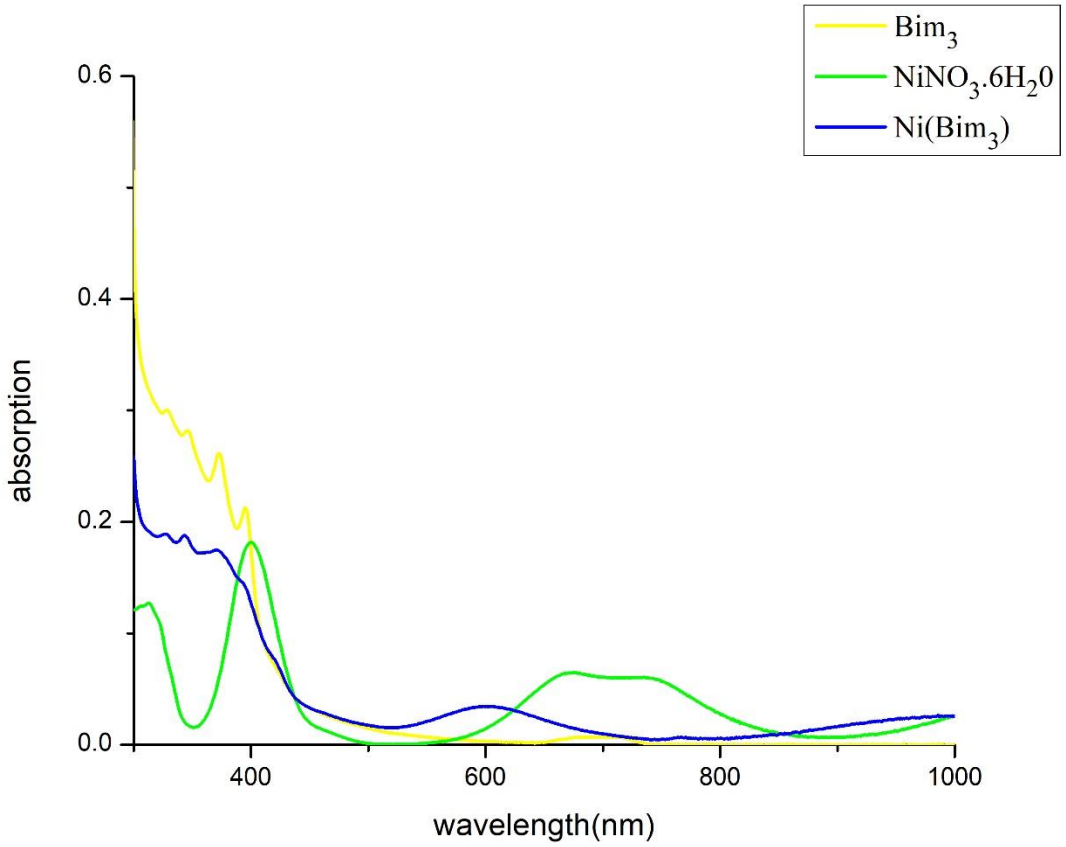

Figure S11: The UV-visible absorption spectra of $(BimH)_3$, **2,** and metal salt recorded in DMF at room temperature.

Table S1: Crystal data and structure refinement for **1**

Empirical formula	$C_{51}H_{51}Cl_3N_{17}Ni_2O_2$	
Formula weight	1157.85	
Temperature/K	273.15	
Wavelength	0.71073 Å	
Crystal system	triclinic	
Space group	P-1	
Unit cell dimensions	a = 11.449(3) Å	α = 103.619(8)°
	b = 12.533(3) Å	β = 94.416(7)°
	c = 19.345(4) Å	γ = 100.604(8)°
Volume	2630.7(10) $Å^3$	
Z	2	
Density(calc)g/cm^3	1.462	
Absorption coefficient/mm^{-1}	0.927	
F(000)	1198.0	
Crystal size	0.08 x 0.15 x 0.12 mm^3	
2 θ range for data collection/°	2.184 to 49.466	
Index ranges	-13 ≤ h ≤ 13, -14 ≤ k ≤ 14, -22 ≤ l ≤ 22	
Reflections collected	55963	
Independent reflections	8925 [R_{int} = 0.1098, R_{sigma} = 0.0768]	
Absorption correction	multi-scan	
Max. and min. transmission	0.7451 and 0.6901	
Refinement methods	Full-matrix least-squares on F^2	
Data/ restraints/ parameters	8925/0/680	
Goodness-of-fit on F^2	1.046	
Final R indices [I>=2σ (I)]	R_1 =0.0682, wR_2 =0.1831	
R indices (all data)	R_1 = 0.1098, wR_2 = 0.2119	
Largest diff. peak and hole	2.73 and -0.78 e $Å^{-3}$	

Table S2: Crystal data and structure refinement for **2a and 2b**

Empirical formula	$C_{2.87}H_{3.18}N_{1.08}Ni_{0.1}O_{0.82}$	
Formula weight	733.32	
Temperature/K	273.15	
Wavelength	0.71073 Å	
Crystal system	triclinic	
Space group	P-1	
Unit cell dimensions	a = 11.067(2) Å	α = 84.047(5)°
	b = 16.567(3) Å	β =89.704(5)°
	c = 17.326(3) Å	γ =84.192(5)°
Volume	3143.4(10) $Å^3$	
Z	39	
Density(calc)g/cm^3	1.482	
Absorption coefficient/mm^{-1}	0.684	
F(000)	1458.0	
Crystal size	0.13 x 0.09 x 0.07 mm^3	
2 θ range for data collection/°	3.602 to 51	
Index ranges	-13 ≤ h ≤ 13, -20 ≤ k ≤ 20, -20 ≤ l ≤ 20	
Reflections collected	55388	
Independent reflections	11679 [R_{int} = 0.0896, R_{sigma} = 0.0860]	
Absorption correction	multi-scan	
Max. and min. transmission	0.7456 and 0.6150	
Refinement methods	Full-matrix least-squares on F^2	
Data/ restraints/ parameters	11679/7/871	
Goodness-of-fit on F^2	1.024	
Final R indices [I>=2σ (I)]	R_1 =0.0531, wR_2 =0.0.1227	
R indices (all data)	R_1 = 0.0828, wR_2 = 0.1409	
Largest diff. peak and hole	0.90 and -0.60 e $Å^{-3}$	

Table S3: Crystal data and structure refinement for **4**

Empirical formula	$C_{28}H_{26}N_{12}NiO_9$	
Formula weight	733.32	
Temperature/K	273.15	
Wavelength	0.71073 Å	
Crystal system	triclinic	
Space group	P-1	
Unit cell dimensions	a =9.7462(16) Å	α =89.766(4)°
	b =10.6213(17) Å	β =74.830(4)°
	c =16.789(3) Å	γ =72.724(4)°
Volume	1596.6(5) $Å^3$	
Z	2	
Density(calc)g/cm^3	1.525	
Absorption coefficient/mm^{-1}	0.681	
F(000)	756.0	
Crystal size	0.11 x 0.15 x 0.09 mm^3	
2 θ range for data collection/°	4.028 to 50.996	
Index ranges	-11 ≤ h ≤ 11, -12 ≤ k ≤ 12, -20 ≤ l ≤ 20	
Reflections collected	25340	
Independent reflections	5049 [R_{int} = 0.0529, R_{sigma} = 0.0422]	
Absorption correction	multi-scan	
Max. and min. transmission	0.745 and 0.683	
Refinement methods	Full-matrix least-squares on F^2	
Data/ restraints/ parameters	5049/0/440	
Goodness-of-fit on F^2	1.036	
Final R indices [I>=2σ (I)]	R_1 =0.0578, wR_2 =0.1518	
R indices (all data)	R_1 = 0.0734, wR_2 = 0.1649	
Largest diff. peak and hole	0.88 and -0.67 e $Å^{-3}$	